

1 **Cloud effects on surface energy and mass balance in the**  
2 **ablation area of Brewster Glacier, New Zealand**

3

4 Manuscript submitted to The Cryosphere Discussions

5 Number of words (main body): 8125

6

7 **J. P. Conway<sup>1,2</sup> and N. J. Cullen<sup>1</sup>**

8 [1]{Department of Geography, University of Otago, Dunedin, New Zealand}

9 [2]{Centre for Hydrology, University of Saskatchewan, Saskatoon, Canada}

10 Correspondence to: J. P. Conway ([jonathan.conway@usask.ca](mailto:jonathan.conway@usask.ca))

11

12 **Keywords:**

13 Energy Balance Obs/Modelling, Alpine Glaciers, Atmospheric Interactions, Southern Alps,  
14 New Zealand

15

16

17

1 **Abstract**

2 The effect of clouds on glacier surface energy balance (SEB) has received increased attention  
3 in the last decade but how clouds interact with other meteorological forcing to influence  
4 surface mass balance (SMB) is not as well understood. This paper resolves the SEB and SMB  
5 at a site in the ablation zone of the Brewster Glacier over a 22-month period, using high  
6 quality radiation data to carefully evaluate SEB terms and define clear-sky and overcast  
7 conditions. A fundamental change in glacier SEB in cloudy conditions was driven by  
8 increased effective sky emissivity and surface vapour pressure, rather than a minimal change  
9 in air temperature and wind speed. During overcast conditions, positive net longwave  
10 radiation and latent heat fluxes allowed melt to be maintained through a much greater length  
11 of time compared to clear-sky conditions, and led to similar melt in each sky condition. The  
12 sensitivity of SMB to changes in air temperature was greatly enhanced in overcast compared  
13 to clear-sky conditions due to more frequent melt and changes in precipitation phase that  
14 created a strong albedo feedback. During the spring and autumn seasons, the sensitivity  
15 during overcast conditions was strongest. To capture these processes, future attempts to  
16 explore glacier-climate interactions should aim to resolve the effects of atmospheric moisture  
17 (vapour, cloud and precipitation) on melt as well as accumulation, through enhanced  
18 statistical or physically based methods.

19

20

# 1 1 Introduction

2 The response of glaciers to atmospheric forcing is of interest as glaciers are seen as useful  
3 scalable proxy records of past climate (e.g. Mölg et al., 2009a) and because the rapid changes  
4 occurring in many glaciated regions have implications for both global sea level rise (Kaser et  
5 al., 2006) and water resources (e.g. Jost et al., 2012). Reliable attribution of past glacier states  
6 and prediction of future ones is dependent on a thorough understanding of the physical  
7 processes operating at the glacier surface that link glacier change with climate, that is, the  
8 surface mass balance (SMB) and surface energy balance (SEB). For debris free, mid-latitude  
9 glaciers, the SMB is primarily a product of the relative magnitudes of accumulated solid  
10 precipitation and melt. While, in general, incoming shortwave radiation ( $SW\downarrow$ ) is the major  
11 source of energy for glacier melt, variations in SMB are considered to be forced by changes in  
12 air temperature and precipitation (Oerlemans, 2005), through both accumulation and melt  
13 processes. Reduced solid precipitation often results in an albedo feedback that increases melt,  
14 thus increased air temperature can result in enhanced melt if the amount of precipitation that  
15 falls as snow decreases. Other mechanisms responsible for the efficient relationship between  
16 air temperature and melt vary widely (Sicart et al., 2008), and include the variability of  
17 turbulent sensible ( $QS$ ) and latent ( $QL$ ) heat fluxes, incoming longwave radiation ( $LW\downarrow$ ), and  
18 a (somewhat spurious) covariance between air temperature and  $SW\downarrow$  in many continental  
19 areas. The primary influence of air temperature on melt rate is also nuanced by other  
20 influences on the SEB such as surface albedo (Oerlemans et al., 2009), humidity (Gillett and  
21 Cullen, 2011), and cloud transmission (Pellicciotti et al., 2005).

22 The strong effect of clouds on glacier SEB has received increased attention in the last decade.  
23 Advances in AWS deployment on glacier surfaces (Mölg et al., 2009b), the availability of  
24 high-quality radiation measurements (van den Broeke et al., 2004), and development of  
25 methods to extract information about cloud cover in data sparse areas (Kuipers Munneke et  
26 al., 2011), have allowed the variation of SEB and SMB with cloud cover to be characterised  
27 in many areas. Sicart et al. (2010) show clouds dominate day to day variations in  $LW\downarrow$  in  
28 mountainous areas while numerous studies detail the fundamental changes in SEB with  
29 cloudiness that are often co-incident with changes in glacier surface boundary layer (SBL)  
30 properties (van den Broeke et al., 2006; Giesen et al., 2008; Gillett and Cullen, 2011). Given  
31 their strong control on the SEB, and coincidence with changes in SBL properties it is vital

1 that the role of clouds in altering the sensitivity of SMB to changes in atmospheric state  
2 variables (especially air temperature) be assessed.

3 The glaciers of the Southern Alps of New Zealand occupy a unique position in the westerly  
4 wind belt of the Southern Ocean, a region dominated by mid-latitude atmospheric circulation  
5 (Tait and Fitzharris, 1998; Ummenhofer and England, 2007). The large barrier the Southern  
6 Alps poses to the prevailing winds creates a high precipitation environment, which, coupled  
7 to the relatively low elevation of glacier termini (Hoelzle et al., 2007), creates high mass  
8 turnover glaciers that have shown high sensitivity to climatic variations in temperature-index  
9 glacier modelling studies (Anderson et al., 2006; Oerlemans, 2010). For these reasons the  
10 glaciers of the Southern Alps are seen as useful indicators of regional atmospheric circulation  
11 in the southwest Pacific and form a vital component of paleoclimate work (e.g. Lorrey et al.,  
12 2007). While a change in precipitation phase and the associated albedo feedback has been  
13 shown to be an important component of the sensitivity of SMB to air temperature in New  
14 Zealand as in other glaciated regions (Oerlemans 1997; Anderson et al., 2006), there is a  
15 suggestion that increased turbulent (mainly sensible) heat fluxes dominate variations in melt  
16 (Anderson et al., 2010). This has led some authors to interpret past glacier fluctuations as a  
17 linear and direct proxy for regional air temperature (e.g. Putnam et al., 2012), at the exclusion  
18 of most other elements of the glacier-climate system.

19 It has been well established that synoptic scale processes exert a strong control on the SMB in  
20 the Southern Alps, with periods of 20<sup>th</sup> century glacier advance and retreat associated with  
21 anomalies in the regional climate system (Fitzharris et al., 2007). Given that this synoptic  
22 variability is closely linked to inferred changes in cloudiness as well as air mass properties  
23 (Hay and Fitzharris, 1988), and that these synoptic controls are thought to have varied over  
24 paleo-climatic timescales (Drost et al., 2007; Ackerley et al., 2011), it is vital that the  
25 influence of clouds on SMB is separated out from the influence of air mass properties (in  
26 particular air temperature). Recent field studies on Brewster Glacier in Southern Alps, have  
27 shown the high frequency of cloudy conditions during all seasons (> 50% overcast  
28 conditions) as well as the significant and variable effect of clouds on  $SW\downarrow$ ,  $LW\downarrow$  and net  
29 radiation ( $R_{net}$ ) (Conway et al., 2014). In this context it is timely to examine in detail the  
30 influence of clouds on glacier surface climate, SEB and melt, as well as the manner in which  
31 clouds alter the sensitivity of SMB to air temperature in the Southern Alps.

1 This paper addresses these issues by resolving the SEB and SMB at a site in the ablation zone  
2 of Brewster Glacier over a 22 month period in 2010 - 2012. High quality surface climate data  
3 presented in Cullen and Conway (2015) are used to force a SMB model (Mölg et al., 2008) to  
4 estimate both SEB and SMB terms over this period (measurement period). The cloud metrics  
5 presented in Conway et al. (2015) are used to identify clear-sky and overcast conditions and  
6 thus characterise surface climate, SEB and melt energy during each condition. To test the  
7 sensitivity of SMB to changes in surface climate and radiative components, a more heavily  
8 parameterised version of the model is used. This model allows us to separate the effects of  
9 changes to surface climate and radiative properties, as well as assess the influence of clouds  
10 on the sensitivity. The sensitivity analyses are run using a two-year time series (sensitivity  
11 period) that was constructed from data collected in the measurement period. The following  
12 section provides a brief description of the site, datasets and modelling methods before the  
13 results and discussion are presented in subsequent sections.

14

## 15 **2 Methods**

### 16 **2.1 Site description and instrumentation**

17 Brewster Glacier is a small mountain glacier situated in the Southern Alps immediately west  
18 of the main divide (Fig. 1). It experiences a temperate maritime high precipitation  
19 environment. Annual precipitation is approximately 6000 mm water equivalent (w.e.), while  
20 the annual air temperature over the glacier surface at 1760 m a.s.l. is 1.2 °C (Cullen and  
21 Conway, 2015). In comparison to other glaciers in the Southern Alps, it has a somewhat lower  
22 average slope (16°) but similar mean and terminus elevation (Hoelzle et al., 2007). As it is  
23 located on the main divide with relatively high exposure to synoptic weather systems, at the  
24 midpoint of the north-south distribution of glaciers in the Southern Alps (Chinn et al., 2012),  
25 it is likely to experience the atmospheric controls on SMB that affect the Southern Alps in  
26 general.

27 [Fig. 1 here]

28 Data from an automatic weather station (AWS) situated in the ablation area of Brewster  
29 Glacier (AWS<sub>glacier</sub>) were used in this study (Fig 1.). Table 1 gives details of instrumentation  
30 and annual average surface climate variables at AWS<sub>glacier</sub>, while further details of the locality

1 and AWS instrumentation can be found in Cullen and Conway (2015). Measurements at  
2 AWS<sub>glacier</sub> ran for 22 months from 25 October 2010 to 1 September 2012 (inclusive). Air  
3 temperature ( $T_a$ ) shows a moderate seasonal cycle (8 °C), and air mass changes appear to  
4 override the subdued diurnal range in  $T_a$ . Wind speed ( $U$ ) is moderate with a persistent down-  
5 glacier flow despite the small fetch and exposed location (Conway, 2013). Humidity is high  
6 with average vapour pressure exceeding that of a melting surface through 4 months during  
7 summer. Cloud cover is frequent and associated with on-glacier wind direction (Conway et  
8 al., 2014). Annual mass balance in the vicinity of AWS<sub>glacier</sub> is generally negative, despite the  
9 large accumulation ( $> 3$  m w.e.) of winter snowfall during May through September. The  
10 significant annual ablation ( $> 4$  m w.e.) generally starts during October, exposing an ice  
11 surface in early January and continuing till April or later.

12 [Table 1 here]

## 13 **2.2 Data treatment and cloud metrics**

14 Cullen and Conway (2015) describe the treatment of the AWS data in detail but a summary of  
15 the main steps is given here. Raw  $T_a$  data were corrected for the overestimation of  $T_a$   
16 measured in the un aspirated shields during times of high solar radiation and low wind speed.  
17 This resulted in a mean correction to the original dataset of  $-0.7^\circ\text{C}$ . To facilitate SMB  
18 modelling, a continuous precipitation dataset ( $P_{scaled}$ ) was constructed by comparing summer  
19 rain gauge observations from a second AWS situated in the pro-glacial area (AWS<sub>lake</sub>) to a  
20 nearby lowland rain gauge ( $R^2 = 0.9$  at a daily level).

21 To construct a high temporal resolution record of observed SMB, surface height observed  
22 using a sonic ranger (Cullen and Conway, 2015) was combined with periodic snow density  
23 measurements. Snow pits near the start of snowmelt indicated a consistent density  
24 approaching  $500 \text{ kg m}^{-3}$  during late October ( $443 \text{ kg m}^{-3}$  on 23 October 2010;  $483 \text{ kg m}^{-3}$  on  
25 27 October 2011), while density during mid-winter was more moderate ( $320 \text{ kg m}^{-3}$  on 18  
26 July 2011). Thus, while the density of melting snow during spring is relatively well  
27 constrained, the increasing density due to subsurface processes (e.g. viscous compaction and  
28 melt – refreezing) during the winter months produces some uncertainty in the relationship  
29 between surface height and SMB. Beyond the snow-ice transition in early January, a standard  
30 ice density of  $900 \text{ kg m}^{-3}$  was assumed, while short periods of new snowfall were assigned a  
31 fresh snow density of  $300 \text{ kg m}^{-3}$  (Gillett and Cullen, 2011).

1 The longwave equivalent cloudiness ( $N\epsilon$ ) used in this study was determined from  
2 measurements of  $LW\downarrow$  and theoretical upper (overcast) and lower (clear-sky) values of  $LW\downarrow$   
3 that are based on surface level meteorological variables, a method that has been used  
4 successfully in other glaciated areas (van den Broeke et al., 2006; Giesen et al., 2008). The  
5 dataset and specific methods used are presented in Conway et al. (2015), but a brief summary  
6 is given below. At each half-hourly interval a theoretical upper limit for  $LW\downarrow$  is set by  
7 applying the Stefan–Boltzmann law to the observed  $T_a$  and an emissivity of 1. A lower limit is  
8 set using the clear-sky model of Konzelmann (1994), which has both  $T_a$  and  $e_a$  as dependant  
9 variables. These two curves are assumed to represent the minimum and maximum  $LW\downarrow$  at a  
10 given  $T_a$  and  $e_a$ , corresponding to cloudiness values of 0 and 1, respectively. By assuming that  
11 cloudiness increases linearly between these minimum and maximum values,  $N\epsilon$  is then  
12 calculated from measured  $T_a$ ,  $e_a$  and  $LW\downarrow$  at each half-hourly interval. Following Giesen et al.  
13 (2008), clear-sky conditions are defined when cloudiness values are smaller than 0.2 and  
14 overcast conditions are defined as cloudiness values larger than 0.8.

15 The inclusion of  $e_a$ , as well as  $T_a$ , as a dependant variable in the calculation of theoretical  
16 clear-sky  $LW\downarrow$  was necessary as clear-sky  $LW\downarrow$  is strongly dependent on both variables at this  
17 temperate location (Durr and Philipona, 2004; Conway et al., 2015). The effect of this is to  
18 include a larger proportion of days in the clear-sky category, as some clear-sky days with high  
19  $e_a$  (and  $LW\downarrow$ ) would have been excluded had only  $T_a$  been used in the calculation of clear-sky  
20  $LW\downarrow$ . A comparison to cloudiness derived from incoming shortwave measurements gave a  
21 correlation coefficient of 0.89 and a root-mean-square-difference (RMSD) of 0.19 (Conway et  
22 al. 2015), suggesting the method is a satisfactory approach to assess cloudiness at this site.

23 Though not directly comparable to traditional cloud fraction metrics based on manual or sky  
24 camera observations,  $N\epsilon$  effectively characterises the impacts of clouds on surface radiation  
25 fluxes. It also has the advantage over metrics based on  $SW\downarrow$ , in that it provides 24 hour  
26 coverage and is not affected by solar zenith angle or multiple reflections between the surface  
27 and atmosphere.

28

29

## 1 2.3 Model description

2 A SMB model (Mölg et al., 2008) was used to resolve surface energy and mass fluxes at  
3 AWS<sub>glacier</sub> for the full 22-month study period. A full description of the model is given in Mölg  
4 et al. (2008, 2009a), but a short description of the parameterisation of each term is given here.  
5 The model computes SMB as the sum of snow accumulation, melt, refreezing of liquid water  
6 in the snowpack and mass fluxes of water vapour (deposition and sublimation) while surface  
7 temperature ( $T_s$ ) is less than 0 °C. Fluxes of vapour while the surface is melting are not  
8 included directly in the SMB as condensation and evaporation add and remove mass from the  
9 liquid melt water at the surface, respectively. The model uses  $T_s$  as a free variable to close the  
10 SEB (equation 1) at each 30-minute timestep:

$$11 \quad QM = SW \downarrow (1 - \alpha) + LW \downarrow - \sigma \varepsilon T_s^4 + QS + QL + QR + QC \quad (1)$$

12 where ( $QM$ ) is the energy for surface melt while  $T_s = 0$  °C,  $SW \downarrow$  is the incoming solar  
13 radiation,  $\alpha$  is the albedo,  $LW \downarrow$  is the incoming longwave radiation,  $\sigma$  is the Stefan-Boltzman  
14 constant ( $5.67 \times 10^{-8}$  W m<sup>-2</sup>),  $\varepsilon$  is the emissivity of snow/ice (equal to unity),  $T_s$  is the surface  
15 temperature (K),  $QS$  and  $QL$  are the turbulent sensible and latent heat fluxes, respectively,  $QR$   
16 is the rain heat flux and  $QC$  is the conductive heat flux through the glacier subsurface. The  
17 convention used is that energy fluxes directed towards the surface are positive.

18 Two different configurations of the model are presented in this paper, distinguished only by  
19 their treatment of surface radiation fluxes. For the first, SEB<sub>mr</sub>, we used measured values of  
20  $SW \downarrow$ ,  $LW \downarrow$  and albedo from AWS<sub>glacier</sub> (Table 2) to provide best estimates of SEB and SMB  
21 terms for analysis over the measurement period. For the second, SEB<sub>pr</sub>, we used  
22 parameterised radiation fluxes (Table 2) to assess the sensitivity of the SMB to changes in  
23 surface climate (detailed further in section 2.5). All other energy fluxes are calculated  
24 consistently between configurations.  $QR$  is calculated using  $P_{scaled}$  assuming rain temperature  
25 is equal to  $T_a$ . New snow was calculated from  $P_{scaled}$  using a rain/snow threshold ( $T_{r/s}$ ) of 1 °C  
26 and a fixed density of 300 kg m<sup>-3</sup>. The iterative SEB closure scheme of Mölg et al. (2008)  
27 was used to calculate  $T_s$ , with  $QC$  being calculated as the flux between the surface and the top  
28 layer of the twelve layer subsurface module (subsurface levels: 0.1, 0.2, 0.3, 0.4, 0.5, 0.8, 1.4,  
29 2, 3, 5, and 7 m). Penetrating shortwave radiation was not included in the model, as the sub  
30 surface temperature profile was not measured throughout the study period, hence the  
31 optimisation of a penetrating shortwave radiation scheme would be subject to large  
32 uncertainty. The depth, density and temperature (iso-thermal at 0 °C) of the snowpack was

1 prescribed at the start of the measurement period from snow-pit measurements (see Sect. 2.2),  
2 while the bottom temperature in the subsurface module was held fixed at 0 °C.

3 [Table 2 here]

4 The turbulent heat fluxes,  $QS$  and  $QL$ , were calculated using a bulk-aerodynamic approach  
5 using the  $C_{log}$  parameterisation as described by Conway and Cullen (2013). The roughness  
6 lengths for momentum ( $z_{0v}$ ), temperature ( $z_{0t}$ ) and humidity ( $z_{0q}$ ) over an ice surface at  
7  $AWS_{glacier}$  are well constrained by in-situ measurements ( $z_{0v} = 3.6 \times 10^{-3}$  m,  $z_{0t} = z_{0q} = 5.5 \times$   
8  $10^{-5}$  m; Conway and Cullen, 2013), though spatial and temporal variability is still probable. A  
9 further period of eddy covariance measurements over a spring snow surface (27 October to 3  
10 November 2011) showed a log-mean value for  $z_{0v}$  of  $1.8 \times 10^{-3}$  m ( $\sigma = 1.3 \times 10^{-2}$  m,  $n = 31$ ),  
11 using the same filtering criterion as Conway and Cullen (2013). No reliable estimates of  $z_{0t}$  or  
12  $z_{0q}$  were possible because of the large uncertainties involved with the small temperature and  
13 vapour pressure gradients experienced during this period. Given the similar, but more  
14 uncertain,  $z_{0v}$  over snow and the large effect of  $z_{0t}$  on the effective roughness length which  
15 tends to counter a change in  $z_{0v}$  (Conway and Cullen, 2013), roughness lengths derived over  
16 ice were adopted for the entire period.

## 17 **2.4 Estimation of uncertainty using a Monte Carlo approach**

18 To estimate uncertainty in modelled SMB, a series of Monte Carlo simulations were made  
19 covering the range of input data and parameter uncertainty expected for each configuration of  
20 the model (SEBmr and SEBpr). Table 3 shows the parameter uncertainty introduced for each  
21 configuration, while input data uncertainty was kept consistent with that used in Conway and  
22 Cullen (2013) and is given in Table 1. For both configurations, 5000 runs of the measurement  
23 period were made, with systematic and random errors being assigned to each input variable  
24 before each simulation and time step, respectively. Errors were calculated by multiplying the  
25 uncertainties associated with each input variable (Tables 1 and 3) by normally distributed  
26 random numbers ( $\mu = 0$ ;  $\sigma = 1$ ), with the exception of  $z_{0v}$  which was logarithmically  
27 transformed before the uncertainty was applied. The 5000 SMB time series computed for each  
28 configuration were subjected to a first order check, using measured  $T_s$  as a proxy for a  
29 realistic simulation of the SEB. Runs were removed when 30-minute modelled  $T_s$  had RMSD  
30  $> 1.5$  K or  $R^2 < 0.9$ , which removed  $\sim 10\%$  of runs from each ensemble. The remaining runs  
31 were then used to compute an ensemble mean and standard deviation for the SMB

1 accumulated over one-day and 10-day periods in addition to the full measurement period.  
2 Runs that did not correctly predict the accumulated SMB at the end of the measurement  
3 period were not removed, as it was unknown if any systematic errors would remain constant  
4 over the study period. Thus, the model uncertainty over a shorter time period (e.g. one or 10  
5 days) was kept independent of the final ‘correct’ accumulated SMB.

6 [Table 3 here]

## 7 **2.5 Mass balance sensitivity configuration**

8 To assess the mass balance sensitivity ( $\Delta\text{SMB}$ ) at  $\text{AWS}_{\text{glacier}}$  further runs were made with the  
9 SEBpr configuration using a hybrid 2-year dataset (sensitivity period). The goal was not only  
10 to show the extent to which elements of the climate system could force SMB changes but also  
11 to understand how uncertainty in model input data or parameterisation impacted estimates of  
12 SMB. Because the measurement period started in spring, the initial depth and density of the  
13 snowpack was prescribed in these runs. However, a realistic evolution of snowdepth with  
14 perturbations in surface climate (especially  $T_a$ ) is required to assess  $\Delta\text{SMB}$ , i.e.  $\Delta\text{SMB}$  is  
15 assessed with accumulation seasons preceding ablation seasons. To this end, a hybrid two-  
16 year dataset was constructed using data from  $\text{AWS}_{\text{glacier}}$  by rearranging the measurement  
17 period timeseries. The particular periods used were (in order): 1 May to 1 September 2012, 2  
18 September to 24 October 2011 and 25 October 2010 to 30 April 2012. This gave two full  
19 SMB seasons (1 May – 30 April) in sensitivity runs and retained variability in the input data  
20 without relying on data from off-glacier sources. Fortunately, the snowdepth predicted by  
21 SEBpr at the end of the first hybrid accumulation season matches that at the start of the  
22 measurement period (25 October 2010) so the evolution of snowdepth (and albedo) during the  
23 remainder of the sensitivity run is comparable with that in the measurement period.

24 To enable the amount of solid precipitation to alter albedo within SEBpr, albedo was  
25 simulated using the parameterisation of Oerlemans and Knap (1998). This scheme computes  
26 albedo from three values representative of fresh snow ( $\alpha_{\text{fresh snow}}$ ), firn ( $\alpha_{\text{firn}}$ ) and ice ( $\alpha_{\text{ice}}$ ),  
27 accounting for the evolution of fresh snow to firn through an e-folding constant ( $t^*$ ) which  
28 describes the characteristic albedo timescale. Two modifications were made to the scheme  
29 (Mölg et al., 2012). Firstly, when new snowfall is removed by melt, the albedo reverts back to  
30 the albedo of the underlying surface. Secondly, a daily total snowfall in excess of 5 cm  
31 (depth) was introduced as a threshold above which the new snowfall impacts albedo, as small

1 snowfall is most likely redistributed into crevasses and hollows on the glacier surface and  
2 have a minimal impact on the albedo.

3 An analysis of measured albedo ( $\alpha_{acc}$ ) at  $AWS_{glacier}$  allowed local values of  $\alpha_{frsnow}$  (0.95),  $\alpha_{firm}$   
4 (0.65) and  $\alpha_{ice}$  (0.42) to be defined (Fig. 2). The higher local values are likely indicative of  
5 lower levels of contaminants that are responsible for reduced albedo at other sites (Oerlemans  
6 et al., 2009) and a lack of debris surrounding Brewster Glacier. A better fit to the evolution of  
7 measured albedo was also found by decreasing  $t^*$  to 10 days, which seems reasonable given  
8 the higher rate of melt (and therefore snow metamorphism) in this maritime environment.  
9 Figure 2 also shows a marked difference in ice surface albedo between the two seasons. It is  
10 unclear if this difference reflects changes over a large spatial scale or if a localised increase in  
11 sediment observed in the vicinity of  $AWS_{glacier}$  during the summer of 2012 contributed to the  
12 decrease in albedo during the second season. Without a clear basis for this variation, a mean  
13 value of  $\alpha_{ice} = 0.42$  was adopted for both seasons.

14 [Fig. 2 here]

15  $\Delta SMB$  was computed by conducting runs with SEBpr over the sensitivity period, introducing  
16 a range of systematic perturbations to input data and parameters (introduced in Sect. 3.4) and  
17 comparing SMB between each run. To calculate variations in  $\Delta SMB$  with cloudiness,  $\Delta SMB$   
18 was computed at each model timestep (i.e. mm w.e. 30-minute<sup>-1</sup>) for each perturbation run.  
19 Model timesteps were then selected based on cloudiness ( $N_c$ ) and a monthly average produced  
20 for clear-sky and overcast conditions. For ease of interpretation,  $\Delta SMB$  was converted to a  
21 daily rate (mm w.e. day<sup>-1</sup>) by multiplying half-hourly  $\Delta SMB$  by the number of model  
22 timesteps within a day (48). By definition, the sum of  $\Delta SMB$  for each timestep within a year  
23 is equal to the accumulated  $\Delta SMB$  of the entire year, which is the more commonly reported  
24 value (e.g. 1.5 m w.e. yr<sup>-1</sup>).

25

## 26 **3 Results**

### 27 **3.1 Model evaluation**

28 Both configurations of the SMB model (SEBmr and SEBpr) were validated against observed  
29  $T_s$  and SMB during the measurement period. Modelled  $T_s$  from reference runs of both  
30 configurations agreed well with  $T_s$  calculated from measurements of outgoing longwave

1 radiation (Fig. 3). Errors at the 30-minute timestep were comparable to other studies (van den  
2 Broeke et al., 2011), and monthly averages indicated no seasonally dependant errors in the  
3 SEB. Both configurations successfully simulated the large accumulation and ablation  
4 observed at AWS<sub>glacier</sub> during the measurement period (Fig. 4). SMB during the first  
5 accumulation season was within  $\pm 10\%$  of that observed (Table 4), which was encouraging  
6 given the uncertainties in the scaled precipitation dataset and rain/snow threshold. SEBmr  
7 showed small discrepancies in modelled ablation (around 10%) for the ice surface in the first  
8 season and the snow surface in the second season (Table 4). SEBpr showed a similar  
9 performance, with an underestimate of ablation for ice surface in the second season likely  
10 related to the lower albedo observed during this season (Fig. 4). Despite these small  
11 deviations, both configurations produced SMBs over the two seasons that were well within  
12 the accumulated uncertainty due to measurement and parameter errors (grey shading in Fig.  
13 4). The small discrepancies between modelled and observed ablation could have been  
14 removed, perhaps through specifying different  $z_{ov}$  for snow and ice surfaces. However, given  
15 the deviations were not consistent between each season and model, both models exhibited  
16 large accumulated uncertainty, and our interest was primarily at shorter timescales, we found  
17 no strong reasoning for tuning model parameters to fit model values precisely.

18 [Fig. 3 here]

19 [Fig. 4 here]

20 [Table 4 here]

21 We also compared SMB over one-day and 10-day periods to ensure we could correctly  
22 simulate the large temporal variability in accumulation and ablation with each configuration  
23 of the model (Fig. 5). SEBmr effectively captured the large variability in SMB during both  
24 accumulation and ablation seasons with maximum 10-day ablation and accumulation rates on  
25 the order of 50 mm w.e. day<sup>-1</sup> (Fig. 5b). A consistent bias in ablation was not observed,  
26 confirming our decision not to tune modelled melt exactly over the season. The significant  
27 number of large daily ablation events ( $> 50$  mm w.e. day<sup>-1</sup>) observed in the ablation record  
28 were, in general, captured by SEBmr (Fig. 5a). If anything, a bias toward under-prediction of  
29 these events was seen. This bias is likely related to an under-prediction of  $QR$ , as the time-  
30 averaging  $P_{scaled}$  underestimated the very intense rainfall rates ( $> 100$  mm day<sup>-1</sup>) associated  
31 with the largest ablation events (Gillett and Cullen, 2011). 10-day accumulation rates were  
32 captured well while daily totals exhibited larger scatter, reflecting the difficulty of

1 determining observed winter SMB from surface height records as well as the large combined  
2 uncertainty due to  $P_{scaled}$ ,  $T_a$  and  $T_{r/s}$ . The good agreement of modelled and observed SMB at  
3 these short temporal resolutions suggests SEBmr is able to capture the variations in melt and  
4 accumulation forced by the key synoptic atmospheric controls.

5 [Fig. 5 here]

6 SEBpr showed similar agreement to observed SMB at both daily and 10-day level (Fig. 5c, d).  
7 The larger uncertainty in modelled ablation was expected given the uncertainties involved in  
8 parameterising incoming radiation fluxes and albedo. A positive bias in modelled ablation  
9 rates was exhibited, though the 1:1 line is still well within the model uncertainty ( $2\sigma$ ). This  
10 bias was likely an artefact of the limited value of the cloud extinction co-efficient ( $k$ ), which  
11 produced a positive bias in ensemble mean  $SW\downarrow$  as compared to the reference run (not  
12 shown). However, this bias was of less concern as the remaining analysis used the reference  
13 run and not the ensemble mean from the Monte Carlo runs to explore cloud effects on SMB  
14 and  $\Delta$ SMB. That the temporal variability of SMB was effectively captured by SEBpr gives us  
15 confidence that this configuration captures the same atmospheric controls on SMB as SEBmr  
16 and as such provides a reliable and useful tool for sensitivity analysis.

### 17 **3.2 Variation of SBL climate with cloudiness**

18 The seasonal variation of surface climate in both clear-sky and overcast conditions during the  
19 measurement period is shown in Figure 6 (a, b). Air temperature ( $T_a$ ) exhibited a clear but  
20 relatively small ( $\sim 8\text{ }^\circ\text{C}$ ) seasonal cycle and was only slightly lower in overcast conditions  
21 compared to clear-sky conditions (Table 5). Vapour pressure ( $e_a$ ) was significantly higher in  
22 overcast conditions, due to the similar  $T_a$  but markedly higher  $RH$ . Consequently in overcast  
23 conditions, mean  $e_a$  was above the saturated vapour pressure of a melting snow/ice surface  
24 (6.11 hPa) during December through April, while in clear-sky conditions mean  $e_a$  only  
25 reached this condition during February. Average  $T_s$  exhibited pronounced differences, being  
26 significantly higher in overcast conditions during every month. Average wind speed ( $U$ ) was  
27 somewhat higher ( $0.1$  to  $0.7\text{ m s}^{-1}$ ) in overcast conditions during most of the ablation season,  
28 while only small or non-significant differences with cloudiness were noted in other seasons  
29 (Table 5). Thus, the main changes in surface climate observed during cloudy periods were an  
30 increase in  $e_a$ , which, despite slightly lower  $T_a$ , were accompanied by a large increase in  $T_s$ .

31 [Table 5 here]

1 [Fig. 6 here]

### 2 **3.3 Variation of SEB and melt with cloudiness**

3 Monthly average SEB terms diagnosed using SEBmr showed marked variation with  
4 cloudiness and season during the measurement period (Fig. 6c, d). Clear-sky conditions were  
5 characterised by large and opposing fluxes.  $SW_{net}$  dominated the seasonal cycle, provided the  
6 largest source of energy during the summer months and peaked after the summer solstice in  
7 response to decreased albedo associated with the transition from a snow to ice surface in early  
8 January.  $LW_{net}$  remained a large sink throughout the year, creating strongly negative  $R_{net}$   
9 during the winter months (JJA) that were responsible for cooling of the glacier surface. Low  
10  $T_s$  in clear-sky conditions allowed  $QS$  to remain directed towards the surface throughout the  
11 year.  $QS$  was of a similar magnitude to  $LW_{net}$  and peaked during the winter months in  
12 response to an increase in both  $U$  and the surface-air temperature gradient (Fig. 6a, b).  $QL$  was  
13 much smaller in magnitude than  $QS$  and of a generally negative sign, indicating that during  
14 clear-skies, sublimation or evaporation dominated over deposition or condensation.  $QR$  was  
15 absent and positive  $QC$  indicated that nocturnal cooling of the surface and subsurface was  
16 occurring.  $QM$  in excess of  $20 \text{ W m}^{-2}$  (equivalent to  $5 \text{ mm w.e. day}^{-1}$ ) was present for a 7-  
17 month period between October and April (inclusive). In general the seasonal cycle of  $QM$   
18 followed that of  $SW_{net}$ , but was modulated by variations in  $QL$  and  $QS$ .

19 In contrast, average energy terms in overcast conditions were smaller in magnitude and  
20 directed towards the surface (Fig. 6d).  $SW_{net}$  was still the largest source of energy to the  
21 surface.  $LW_{net}$  was positive through most of the year, due to the enhancement of  $LW_{\downarrow}$  by low  
22 cloud cover and the  $T_s$  being limited to  $0 \text{ }^{\circ}\text{C}$ . Consequently,  $R_{net}$  was positive throughout the  
23 year and larger than in clear-sky conditions from March to November (inclusive).  $QS$  and  $QL$   
24 were nearly equal in magnitude and both directed towards the surface, together producing a  
25 source of energy comparable to the contribution from  $R_{net}$ . A distinct seasonal cycle in  $QS$   
26 and  $QL$  was driven by the strong seasonal variation in surface-air temperature and moisture  
27 gradients in overcast conditions (Fig. 6b).  $QR$  made a small contribution to  $QM$  during the  
28 summer and  $QC$  was negligible. The net result was that despite the moderate magnitude of  
29 individual energy fluxes in overcast conditions, mean  $QM$  was similar to values observed in  
30 clear-sky conditions during most months. The exception was between February and May,  
31 where  $QM$  in overcast conditions exceeded values in clear-sky conditions.

1 While mean  $QM$  was similar in clear-sky and overcast conditions, melting occurred much  
2 more frequently in overcast conditions (Fig. 7). Given that day length varies between 11.5 and  
3 15.5 hours during October through April (inclusive) and that melt occurred during 70% to  
4 95% of overcast conditions, nocturnal melt was a significant feature in overcast conditions  
5 during these months. While clear-sky and overcast conditions accounted for 36% and 45% of  
6 the measurement period, respectively (Conway et al., 2015), they were responsible for 30%  
7 and 50% of total melt, respectively, simply because melt occurred more frequently in overcast  
8 conditions.

9 [Fig. 7 here]

10 [Table 6 here]

11 When all melting periods were considered together (42% of measurement period),  $SWnet$   
12 made the largest contribution to  $QM$ , with  $QS$  and  $QL$  together contributing a little over one  
13 third and  $QR$  providing a non-negligible fraction (Table 6). On average,  $LWnet$  and  $QC$  were  
14 energy sinks during melting periods. Considering the average SEB terms during all periods, a  
15 shift towards  $QS$  at the expense of  $Rnet$  was observed, due to the inclusion of non-melting  
16 clear-sky periods where negative  $LWnet$  was largely balanced by  $QS$ .

### 17 **3.4 Sensitivity of SMB to surface climate**

18 Model runs with SEBpr over the sensitivity period (see Sect. 2.4) highlight the large  
19 sensitivity of SMB to  $T_a$  (Table 7). The mass balance sensitivity ( $\Delta SMB$ ) is defined as the  
20 average change in SMB per annum for both positive and negative perturbations in each  
21 climate variable. For clarity,  $\Delta SMB$  is expressed as the SMB response to an increase in a  
22 given input variable or parameter. The modest change in SMB to  $P_{scaled} \pm 20\%$  indicates an  
23 extremely large increase in precipitation would be needed to offset the mass loss associated  
24 with moderate atmospheric warming. Increased  $RH$  induces a small mass loss, due to  
25 increased  $LW\downarrow$  and  $QL$ . Similarly, a mass loss of 0.79 m w.e.  $yr^{-1}$  occurs for a 1 m  $s^{-1}$  increase  
26 in  $U$ , due to an increased contribution of turbulent heat fluxes to melt. The  $\Delta SMB$  to terms  
27 controlling  $SWnet$  is high, with  $\alpha \pm 0.1$  inducing over half the SMB response of  $T_a \pm 1$  K  
28 (Table 7). Variations in the cloud extinction coefficient ( $k$ ), within the uncertainty range of the  
29 radiation scheme optimisation (Conway et al., 2015), induce large changes in SMB,  
30 emphasizing the important contribution of  $SWnet$  to melt during overcast conditions (Table

1 6). A 6% decrease in  $SW_{TOA}$  (the approximate change in the solar constant during the last  
2 10,000 years) results in only a modest mass loss.

3 [Table 7 here]

4 To examine how the large  $\Delta SMB$  to  $T_a$  is expressed, a breakdown of SMB terms was  
5 constructed for the +1 K and -1 K perturbation runs (Table 8). A change in snowfall accounts  
6 for 21% of  $\Delta SMB$ , while a small change in refreezing (2%) and a dominant change in melt  
7 (77%) account for the remainder. Changes in deposition and sublimation are negligible. It is  
8 worth clarifying here that changes in snowfall resulting from the perturbations in  $T_a$  in this  
9 analysis are due solely to changes in the fraction of precipitation falling as snow versus rain.  
10 This is distinct from the atmospheric feedback between air temperature and precipitation that  
11 can result in increased accumulation due to enhanced precipitation rates in a warmer climate  
12 (e.g. Box et al., 2012). The temperate nature of the glacier SBL in the vicinity of  $AWS_{glacier}$   
13 increases the  $\Delta SMB$  to  $T_a$  as most precipitation falls within a few degrees of the rain/snow  
14 threshold and snowfall can occur at any time of the year (Cullen and Conway, 2015). Indeed,  
15 despite the large ablation at  $AWS_{glacier}$  over the 22 month measurement period ( $> 9$  m w.e.), a  
16 decrease in  $T_a$  of 1.3 K would be sufficient to produce a net zero SMB.

17 [Table 8 here]

18 The change in melt between  $T_a$  perturbation runs can be attributed to SEB components whose  
19 magnitude is either directly dependent on  $T_a$  (i.e.  $LW_{\downarrow}$ ,  $QS$ ,  $QL$ , and  $QR$ ), or indirectly altered  
20 by changes to melt and/or snowfall that alter albedo (i.e.  $SW_{net}$ ). Table 9 shows mean SEB  
21 components for each  $T_a$  perturbation run. The most striking feature is that while a 100%  
22 increase in melt occurs between -1 K and +1 K runs (Table 8), there is only a 40% increase in  
23  $QM$  during melt (Table 9, A & B final column). The majority of increased melt is due to a  
24 large increase in the fraction of time melt occurs, from 34% to 48% of all periods. Thus, a  
25 better indication of the contribution of each SEB term to  $\Delta SMB$  can be found by examining  
26 the change in SEB terms between runs for the melting periods in the + 1 K run, (Table 9, E).  
27 By multiplying the contribution of each SEB term to the increase in melt by the fraction melt  
28 contributes to the total  $\Delta SMB$  (77%; Table 8), we find the contribution of each SEB term to  
29 the  $\Delta SMB$  (Table 9, F).  $SW_{net}$  makes the largest contribution to the increase in melt and  
30 accounts for over one third of the  $\Delta SMB$ . The turbulent heat fluxes,  $QS$  and  $QL$ , together  
31 account for less than a third of the  $\Delta SMB$ , while  $LW_{net}$  and  $QR$  make smaller contributions.  
32 Thus, changes in  $QM$  that are directly dependent on  $T_a$  contribute less than half of the  $\Delta SMB$ ,

1 while changes in snow accumulation and the albedo feedback account for the majority. Given  
2 the covariance of cloudiness and SEB terms shown in Sect. 3.3 and the obvious link between  
3 cloudiness and precipitation, further examination of the interplay between cloudiness and  
4  $\Delta\text{SMB}$  is made in the following section.

5 [Table 9 here]

### 6 **3.5 Impact of clouds on SMB sensitivity**

7 To begin to describe the influence of cloud cover on the relationship between SMB and  $T_a$ ,  
8 the amount of melt that occurred under clear-sky, partial cloud and overcast conditions was  
9 calculated for each  $T_a$  perturbation run (Fig. 8). Overcast periods exhibit the largest change in  
10 melt between  $T_a$  perturbation runs, accounting for 50% of the  $\Delta\text{SMB}$  to  $T_a$ . Clear-sky and  
11 partial cloud conditions show more modest changes in melt and account for 29% and 21% of  
12 the  $\Delta\text{SMB}$ , respectively. By calculating the mean  $\Delta\text{SMB}$  in clear-sky and overcast conditions  
13 for each month, a distinct seasonal cycle as well as a clear dependence on cloudiness emerged  
14 (Fig. 9). In general, the  $\Delta\text{SMB}$  is greatly reduced during winter months, as  $T_a$  is well below  
15  $T_{r/s}$  and ablation is minimal at  $\text{AWS}_{\text{glacier}}$ . Overcast conditions almost always produce higher  
16  $\Delta\text{SMB}$  than clear-skies, especially during spring and autumn. A peak in  $\Delta\text{SMB}$  during  
17 October is associated with a higher fraction of marginal melt conditions and average  $T_a$   
18 around  $T_{r/s}$ . From May through October (inclusive)  $\Delta\text{SMB}$  in clear-sky conditions is minimal.  
19 January and February, however, show large  $\Delta\text{SMB}$  in clear-sky conditions, as the magnitude  
20 of  $\text{SW}_{\text{net}}$  during these months is greatly influenced by changes in albedo driven by the timing  
21 of the transition to an ice surface and occurrence of summer snowfall. This albedo feedback  
22 occurs as increased  $T_a$  decreases the fraction of precipitation falling as snow, thus decreasing  
23 the duration of snow cover and reducing summer snowfall.

24 In order to remove the albedo feedback, further runs of SEBpr were made for - 1 K and + 1 K  
25 scenarios. By using measured albedo and perturbing  $T_{r/s}$  by the same magnitude as  $T_a$ , both  
26 accumulation and  $\text{SW}_{\text{net}}$  remained consistent between these runs and the resulting  $\Delta\text{SMB}$   
27 (direct) is due to only changes in  $QM$  directly caused by increased  $T_a$  (Fig. 9., dashed lines).  
28 The divergence of full and direct  $\Delta\text{SMB}$  in clear-skies conditions confirmed that changes in  
29 melt due to an albedo feedback dominate clear-sky  $\Delta\text{SMB}$ , especially in the summer. In  
30 overcast conditions, the direct  $\Delta\text{SMB}$  is somewhat less than the full  $\Delta\text{SMB}$  in each month, as  
31 periods with altered snowfall are removed. Still, the direct  $\Delta\text{SMB}$  remained approximately

1 twice as large as that in clear-sky conditions through each month. Thus, it is evident that  
2 cloudy conditions have a much stronger influence on  $\Delta\text{SMB}$  to  $T_a$  than clear-sky conditions,  
3 with an increased  $\Delta\text{SMB}$  in cloudy conditions being due to changes in both snowfall and melt,  
4 and being strongest in the spring and autumn seasons.

5 [Fig. 8 here]

6 [Fig. 9 here]

## 7 **4 Discussion**

### 8 **4.1 Cloud impacts on SBL and SEB**

9 The large difference in SEB terms between clear and overcast conditions seen in these results  
10 is driven in large part by changes in  $e_a$ , rather than changes in  $T_a$ . The increase in  $e_a$  in  
11 overcast conditions is enabled by the poor association of  $T_a$  and cloud cover, in addition to the  
12 obvious covariance between  $RH$  and cloudiness. That  $T_a$  is not markedly decreased in  
13 overcast conditions differs from similar studies in the European Alps (e.g. Pellicciotti et al.,  
14 2005) and Norway (Giesen et al., 2008), and is indicative of the maritime setting where  
15 air mass properties, rather than a positive association between summertime insolation and air  
16 temperature (Sicart et al., 2008), are the primary control on SBL variations (Cullen and  
17 Conway, 2015). The availability of moist and relatively warm air masses to the glacier surface  
18 also creates positive  $LW_{net}$  in overcast conditions, which along with increases in  $QL$ , allows  
19 for steady melt through much greater periods of time. Consequently, average daily melt rates  
20 are similar in clear-sky and overcast conditions, again in contrast with studies in the European  
21 Alps that show increased melt in clear-sky conditions (Pellicciotti et al., 2005). Glaciers in  
22 Norway (Giesen et al., 2008) show higher total melt during overcast conditions due to higher  
23  $U$  that increase turbulent heat fluxes during frequent cloud cover. While increased  $U$  and  
24 turbulent heat fluxes are observed for the largest melt events on Brewster Glacier (Gillett and  
25 Cullen, 2011), mean  $U$  was not well differentiated by cloudiness over the measurement  
26 period, leaving  $T_a$  and  $e_a$  as the primary controls of mean  $QS$  and  $QL$ , respectively.

27 While  $LW_{net}$  was substantially increased during overcast periods, a ‘radiation paradox’  
28 (Ambach, 1974) does not occur during most of the melt season in the ablation zone of  
29 Brewster Glacier, due to high  $SW_{TOA}$ , large cloud extinction coefficients and a smaller  
30 difference in sky emissivity in clear-sky and overcast conditions at this mid-latitude location.  
31 In contrast, maritime sites on the melting margin of the Greenland ice sheet show clouds act

1 to increase  $R_{net}$  throughout the melt season at a range of elevations (van den Broeke et al.,  
2 2008a). At the lowest site where the surface is melting over 80% of the summer period, the  
3 presence of a strong ‘radiation paradox’ implies that melt rates are higher during overcast  
4 conditions, which is supported by the absence of increased summer melt during more frequent  
5 clear-sky conditions (van den Broeke et al., 2011). The lack of a ‘radiation paradox’ during  
6 the summer months on the lower part of Brewster Glacier emphasises the role of air mass  
7 properties that are advected from the surrounding ocean areas in maintaining  $T_a$  and enabling  
8 enhanced  $LW_{net}$  and  $QL$  during overcast periods. In the same way, during the transition  
9 periods, especially in the autumn, increased melt rates were enabled by a ‘radiation paradox’.

## 10 **4.2 Cloud impacts on SMB sensitivity**

11 The increased sensitivity of SMB to  $T_a$  in overcast conditions may help explain some of the  
12 high sensitivity of SMB to  $T_a$  in the Southern Alps. Importantly, average melt is not reduced  
13 in overcast conditions and cloud cover is frequent in the Southern Alps. Therefore, a large  
14 fraction of melt occurs in overcast conditions which the results from this research suggest are  
15 more sensitive to changes in  $T_a$ . In conjunction with increased  $e_a$ , clouds extend melt into  
16 periods of marginal melt that are more sensitive to changes in  $T_a$ , as well as being strongly  
17 associated with frequent precipitation around  $T_{r/s}$ . Indeed, roughly half of the sensitivity to  $T_a$   
18 is due to an albedo feedback, in line with previous work in the Southern Alps (Oerlemans,  
19 1997), emphasising the turbulent heat fluxes play a secondary role, despite the assertions of  
20 recent paleo-climatic research (Putnam et al., 2012). In addition, the largest melt events –  
21 which constitute a large fraction of melt over a season (Gillett and Cullen, 2011) – are  
22 associated with overcast conditions and contribute to proportionally larger changes in melt.  
23 Thus, air mass variability, in particular air temperature associated with high water vapour  
24 content, appears to be the primary control on melt during the summer ablation season.

25 Aside from their role in the  $\Delta\text{SMB}$  to  $T_a$ , the contribution of turbulent heat fluxes to melt may  
26 have been overstated in a number of studies, at the expense of  $R_{net}$ . In fact, the contribution  
27 of  $R_{net}$  to ablation in the present study is similar to that found over mixed snow/ice ablation  
28 surfaces in Norway (68%; Giesen et al., 2008) and coastal Greenland ( $\sim 70\%$  (S6); van den  
29 Broeke et al., 2008b), and similar to that found for a neve area in New Zealand (Kelliher et  
30 al., 1996). There are a number of possible reasons for the deviation of the current study from  
31 previously reported values for glacier surfaces in the Southern Alps (e.g. Marcus et al., 1985;  
32 Hay and Fitzharris, 1988; Ishikawa et al., 1992; Anderson et al., 2010). Firstly, in earlier

1 studies simplifications were usually made in the calculation of the turbulent heat fluxes,  
2 including the assumption that the surface is always melting. Secondly, average SEB terms  
3 were traditionally reported for the entire study period, rather than only those during periods of  
4 melt. Table 6 clearly shows full-period average SEB terms are biased towards  $QS$ , as non-  
5 melting nocturnal and winter periods are included. These periods have higher values of  $QS$ ,  
6 which serve to balance negative  $LW_{net}$ . Lastly, a number of the studies have been conducted  
7 in low elevation areas, where turbulent heat fluxes are increased, despite these areas being  
8 atypical in the Southern Alps (mean elevation of glacier termini  $> 1500$  m a.s.l.; Hoelzle et  
9 al., 2007).

### 10 **4.3 Implications for modelling glacier-climate interactions**

11 While the present study does not make an assessment of glacier wide  $\Delta$ SMB and therefore is  
12 somewhat limited in discussing atmospheric controls on glacier fluctuations, it shows that the  
13 response of glacier melt to changes in  $T_a$  can be altered by clouds. This has two important  
14 implications for our understanding of glacier climate interactions.

15 Firstly, efforts to characterise glacier-climate connections need to consider the effects of  
16 changing atmospheric moisture on melt rate as well as accumulation. New avenues to model  
17 glacier melt with enhanced temperature index models (TIM) or other empirical descriptions of  
18 the temperature dependant fluxes (e.g. Giesen and Oerlemans, 2012) need to consider the  
19 variance of atmospheric moisture with respect to melt. This is both due to the strong increase  
20 in  $LW_{\downarrow}$  by clouds, but also the association with increased positive  $QL$  in moist environments.  
21 This may be important for other maritime areas, as well as the Southern Alps where TIM's  
22 have already been shown to break down in large melt events (Cutler and Fitzharris, 2005;  
23 Gillett and Cullen, 2011). The use of coupled glacier mass balance – atmospheric models also  
24 present an avenue to represent past and future interactions in a physically realistic way (e.g.  
25 Collier et al. 2013).

26 Secondly, it follows that a change in the frequency of cloud cover or synoptic regime may  
27 enhance/dampen the SMB response to  $T_a$ . For example, a decrease in  $\Delta$ SMB from west to east  
28 across the Southern Alps is likely, in association with the strong gradient of precipitation and  
29 cloudiness (Uddstrom et al., 2001). It is enticing to reduce the relationship between glacier  
30 mass balance and climate to the main causal mechanisms (i.e. temperature / precipitation  
31 paradigm). However, there is also the possibility that changes in atmospheric circulation

1 coincident with changes in state variables in the past (i.e. during the last glacial maximum;  
2 Drost et al., 2007; Ackerley et al., 2011) may alter empirical relationships (i.e. TIM's)  
3 informed during the present climate, altering the climate signals derived from glacier  
4 fluctuations. For the Southern Alps, the most compelling analysis of the controls on SMB  
5 points to changes in the regional circulation patterns (Fitzharris et al., 2007), which are in turn  
6 associated with strong changes in both air mass properties and cloudiness (Hay and Fitzharris,  
7 1988). Thus, it is likely that average relationships between melt and air temperature may  
8 indeed be changed if a shift to drier or wetter conditions is experienced.

9 The high fraction of melt due to  $SW_{net}$  and large contribution of an albedo feedback to  $\Delta SMB$   
10 also implies that local or regional influences on albedo may have an important role in  
11 modifying melt rate as seen in other areas (Oerlemans et al., 2009). Indeed, the LGM period  
12 shows higher rates of glacial loess deposition in New Zealand (Eden and Hammond, 2003),  
13 thus the role of terrigenous dust in modifying glacier ablation rates during the onset of glacier  
14 retreat (e.g. Peltier and Marshall, 1995) is a topic that should be explored further in the  
15 context of the Southern Alps.

16

## 17 **5 Conclusions**

18 We have presented a validated timeseries of SEB/SMB in the ablation zone of a glacier in the  
19 Southern Alps of New Zealand during 2 annual cycles. High quality radiation data allowed a  
20 careful evaluation of the magnitude of SEB terms, as well as the selection of clear-sky and  
21 overcast conditions. An analysis of SBL climate and SEB showed a fundamental change in  
22 SEB with cloudiness that was driven by an increase in effective sky emissivity and vapour  
23 pressure at the glacier surface. The only slightly diminished  $T_a$  during overcast periods  
24 created positive  $LW_{net}$  and also allowed both  $QS$  and  $QL$  to remain large and directed toward  
25 the surface. This created a strong increase in the fraction of time the surface was melting in  
26 overcast conditions, which led to a similar average melt rate in clear-sky and overcast  
27 conditions. Given the frequent cloud cover at the site, cloudy periods accounted for a majority  
28 of the melt observed, especially during autumn when  $SW_{net}$  inputs were lower.

29 A parameterisation of radiation components allowed the sensitivity of SMB to independent  
30 changes in SBL climate and shortwave radiation components to be assessed. The large  
31 sensitivity of SMB to  $T_a$  was expressed primarily through changes in the partitioning of  
32 precipitation into snowfall and rainfall, as well as the associated albedo feedback. The

1 remainder of this sensitivity was due to changes in the fraction of time the surface was  
2 melting and changes in the magnitude of  $QS$ ,  $QL$ ,  $LW_{net}$  and  $QR$  (in that order of  
3 importance). The sensitivity of SMB to  $T_a$  diverged strongly when partitioned into clear-sky  
4 and overcast periods. Enhanced sensitivity was found in overcast periods due to the  
5 occurrence of precipitation and an ability for melt to be produced over larger fractions of  
6 time. Increased sensitivity during overcast periods may explain some of the high sensitivity of  
7 SMB in the Southern Alps, and raises the possibility that the response of SMB to  $T_a$  in the  
8 past or future may be altered by changing synoptic patterns that are strongly associated with  
9 cloud cover. Thus, it highlights the need to include the effect of atmospheric moisture  
10 (vapour, cloud and precipitation) on both melt and accumulation processes when modelling  
11 glacier-climate interactions.

12

### 13 **Acknowledgements**

14 Funding from a University of Otago Research Grant (ORG10-10793101RAT) supported N.  
15 Cullen's contribution to this research. The research also benefited from the financial support  
16 of the National Institute of Water and Atmospheric Research, New Zealand (Climate Present  
17 and Past CLC01202), and collaboration with A. Mackintosh and B. Anderson, Victoria  
18 University of Wellington. The Department of Conservation supported this research under  
19 concession OT-32299-OTH. We thank T. Mölg for providing model code and for many  
20 helpful discussions on model development, as well as P. Sirguey and W. Colgan for helpful  
21 discussions on the Monte Carlo approach. D. Howarth and N. McDonald provided careful  
22 technical support for the field measurements.

23

## 1 **References**

- 2 Ackerley, D., Lorrey, A., Renwick, J. A., Phipps, S. J., Wagner, S., Dean, S., Singarayer, J.,  
3 Valdes, P., Abe-Ouchi, A., Ohgaito, R. and Jones, J. M.: Using synoptic type analysis to  
4 understand New Zealand climate during the Mid-Holocene, *Clim. Past*, 7(4), 1189–1207,  
5 doi:10.5194/cp-7-1189-2011, 2011.
- 6 Ambach, W.: The influence of cloudiness on the net radiation balance of a snow surface with  
7 high albedo, *J. Glaciol.*, 13(67), 73–84, 1974.
- 8 Anderson, B., Lawson, W., Owens, I. and Goodsell, B.: Past and future mass balance of “Ka  
9 Roimata o Hine Hukatere” Franz Josef Glacier, New Zealand, *J. Glaciol.*, 52(179), 597–607,  
10 doi:10.3189/172756506781828449, 2006.
- 11 Anderson, B., Mackintosh, A., Stumm, D., George, L., Kerr, T., Winter-Billington, A. and  
12 Fitzsimons, S.: Climate sensitivity of a high-precipitation glacier in New Zealand, *J. Glaciol.*,  
13 56(195), 114–128, doi:10.3189/002214310791190929, 2010.
- 14 Blonquist, J. M., Tanner, B. D. and Bugbee, B.: Evaluation of measurement accuracy and  
15 comparison of two new and three traditional net radiometers, *Agric. For. Meteorol.*, 149(10),  
16 1709–1721, doi:10.1016/j.agrformet.2009.05.015, 2009.
- 17 Box, J.E., Fettweis, X., Stroeve, J.C., Tedesco, M., Hall, D. K., and Steffen, K.: Greenland ice  
18 sheet albedo feedback: thermodynamics and atmospheric drivers, *Cryosph.*, 6, 821–839, doi:  
19 10.5194/tc-6-821-2012, 2012.
- 20 Chinn, T., Fitzharris, B. B., Willsman, A. and Salinger, M. J.: Annual ice volume changes  
21 1976–2008 for the New Zealand Southern Alps, *Glob. Planet. Change*, 92–93, 105–118,  
22 doi:10.1016/j.gloplacha.2012.04.002, 2012.
- 23 Collier, E., Mölg, T., Maussion, F., Scherer, D., Mayer, C. and Bush, A. B. G.: High-  
24 resolution interactive modelling of the mountain glacier–atmosphere interface: an application  
25 over the Karakoram, *Cryosph.*, 7(3), 779–795, doi:10.5194/tc-7-779-2013, 2013.
- 26 Conway, J. P.: Constraining Cloud and Airmass Controls on the Surface Energy and Mass  
27 Balance of Brewster Glacier, Southern Alps of New Zealand (Thesis, Doctor of Philosophy),  
28 University of Otago, <http://hdl.handle.net/10523/4432> (last access: 1 December 2014), 2013.
- 29 Conway, J. P. and Cullen, N. J.: Constraining turbulent heat flux parameterization over a  
30 temperate maritime glacier in New Zealand, *Ann. Glaciol.*, 54(63), 41–51,  
31 doi:10.3189/2013AoG63A604, 2013.
- 32 Conway, J. P., Cullen, N. J., Spronken-Smith, R. A., and Fitzsimons, S. J.: All-sky radiation  
33 over a glacier surface in the Southern Alps of New Zealand: characterizing cloud effects on  
34 incoming shortwave, longwave and net radiation, *Int. J. Climatol.*, 35, 699–713,  
35 doi:10.1002/joc.4014, 2015.
- 36 Cullen, N. J. and Conway, J. P.: A 22-month record of surface meteorology and energy  
37 balance from the ablation zone of Brewster Glacier, New Zealand, *J. Glaciol.*, in press, 2015.

- 1 Cutler, E. S. and Fitzharris, B.: Observed surface snowmelt at high elevation in the Southern  
2 Alps of New Zealand, *Ann. Glaciol.*, 40(1), 163–168, doi:10.3189/172756405781813447,  
3 2005.
- 4 Drost, F. and Renwick, J.: Simulation of New Zealand's climate using a high-resolution  
5 nested regional climate model, *Int. J. Climatol.*, 1169, 1153–1169, doi: 10.1002/joc.1461,  
6 2007.
- 7 Dürr, B. and Philipona, R.: Automatic cloud amount detection by surface longwave  
8 downward radiation measurements, *J. Geophys. Res.*, 109(D5), D05201,  
9 doi:10.1029/2003JD004182, 2004.
- 10 Eden, D. N. and Hammond, A. P.: Dust accumulation in the New Zealand region since the  
11 last glacial maximum, *Quat. Sci. Rev.*, 22(18-19), 2037–2052, doi:10.1016/S0277-  
12 3791(03)00168-9, 2003.
- 13 Fitzharris, B. B., Clare, G. R. and Renwick, J. A.: Teleconnections between Andean and New  
14 Zealand glaciers, *Glob. Planet. Change*, 59(1-4), 159–174,  
15 doi:10.1016/j.gloplacha.2006.11.022, 2007.
- 16 Giesen, R. H., van den Broeke, M. R., Oerlemans, J. and Andreassen, L. M.: Surface energy  
17 balance in the ablation zone of Midtdalsbreen, a glacier in southern Norway: Interannual  
18 variability and the effect of clouds, *J. Geophys. Res.*, 113(D21), 1–17,  
19 doi:10.1029/2008JD010390, 2008.
- 20 Giesen, R. H. and Oerlemans, J.: Calibration of a surface mass balance model for global-scale  
21 applications, *Cryosph.*, 6(6), 1463–1481, doi:10.5194/tc-6-1463-2012, 2012.
- 22 Gillett, S. and Cullen, N. J.: Atmospheric controls on summer ablation over Brewster Glacier,  
23 New Zealand, *Int. J. Climatol.*, 31(13), 2033–2048, doi:10.1002/joc.2216, 2011.
- 24 Hay, J. E. and Fitzharris, B. B.: The synoptic climatology of ablation on a New Zealand  
25 glacier, *J. Climatol.*, 8(2), 201–215, doi:10.1002/joc.3370080207, 1988.
- 26 Hoelzle, M., Chinn, T., Stumm, D., Paul, F., Zemp, M. and Haeberli, W.: The application of  
27 glacier inventory data for estimating past climate change effects on mountain glaciers: A  
28 comparison between the European Alps and the Southern Alps of New Zealand, *Glob. Planet.*  
29 *Change*, 56(1-2), 69–82, doi:10.1016/j.gloplacha.2006.07.001, 2007.
- 30 Ishikawa, N., Owens, I. F. and Sturman, A. P.: Heat balance characteristics during find  
31 periods on the lower parts of the Franz Josef Glacier, South Westland, New Zealand, *Int. J.*  
32 *Climatol.*, 12, 397–410, 1992.
- 33 Jost, G., Moore, R. D., Menounos, B. and Wheate, R.: Quantifying the contribution of glacier  
34 runoff to streamflow in the upper Columbia River Basin, Canada, *Hydrol. Earth Syst. Sci.*,  
35 16(3), 849–860, doi:10.5194/hess-16-849-2012, 2012.

- 1 Kaser, G., Cogley, J. G., Dyurgerov, M. B., Meier, M. F. and Ohmura, A.: Mass balance of  
2 glaciers and ice caps: Consensus estimates for 1961–2004, *Geophys. Res. Lett.*, 33(19),  
3 L19501, doi:10.1029/2006GL027511, 2006.
- 4 Kelliher, F. M., Owens, I. F., Sturman, A. P., Byers, J. N., Hunt, J. E. and McSeveny, T. M.:  
5 Radiation and ablation on the neve of Franz Josef Glacier, *J. Hydrol.*, 35(1), 129–148, 1996.
- 6 Konzelmann, T., Van de Wal, R., Greuell, W., Bintanja, R., Henneken, E. and Abe-Ouchi, A.:  
7 Parameterization of global and longwave incoming radiation for the Greenland Ice Sheet,  
8 *Glob. Planet. Change*, 9, 143–164, 1994.
- 9 Kuipers Munneke, P., Reijmer, C. H. and van den Broeke, M. R.: Assessing the retrieval of  
10 cloud properties from radiation measurements over snow and ice, *Int. J. Climatol.*, 31(5),  
11 756–769, doi:10.1002/joc.2114, 2011.
- 12 Lorrey, A., Fowler, A. M. and Salinger, J.: Regional climate regime classification as a  
13 qualitative tool for interpreting multi-proxy palaeoclimate data spatial patterns: A New  
14 Zealand case study, *Palaeogeogr. Palaeoclimatol. Palaeoecol.*, 253(3-4), 407–433,  
15 doi:10.1016/j.palaeo.2007.06.011, 2007.
- 16 Machguth, H., Purves, R. S., Oerlemans, J., Hoelzle, M. and Paul, F.: Exploring uncertainty in  
17 glacier mass balance modelling with Monte Carlo simulation, *Cryosph.*, 2, 447–485,  
18 doi:10.5194/tcd-2-447-2008, 2008.
- 19 Marcus, M. G., Moore, R. D. and Owens, I. F.: Short-term estimates of surface energy  
20 transfers and ablation on the lower Franz Josef Glacier, South Westland, New Zealand, *New  
21 Zeal. J. Geol. Geophys.*, 28, 559–567, 1985.
- 22 Mölg, T., Cullen, N., Hardy, D. R., Kaser, G. and Klok, L.: Mass balance of a slope glacier on  
23 Kilimanjaro and its sensitivity to climate, *Int. J. Climatol.*, 28, 881–892, doi:10.1002/joc1589,  
24 2008.
- 25 Mölg, T., Cullen, N. J., Hardy, D. R., Winkler, M. and Kaser, G.: Quantifying Climate  
26 Change in the Tropical Midtroposphere over East Africa from Glacier Shrinkage on  
27 Kilimanjaro, *J. Clim.*, 22(15), 4162–4181, doi:10.1175/2009JCLI2954.1, 2009a.
- 28 Mölg, T., Cullen, N. and Kaser, G.: Solar radiation, cloudiness and longwave radiation over  
29 low-latitude glaciers: implications for mass-balance modelling, *J. Glaciol.*, 55(190), 292–302,  
30 2009b.
- 31 Mölg, T., Großhauser, M., Hemp, A., Hofer, M. and Marzeion, B.: Limited forcing of glacier  
32 loss through land-cover change on Kilimanjaro, *Nat. Clim. Chang.*, 2(4), 254–258,  
33 doi:10.1038/nclimate1390, 2012.
- 34 Oerlemans, J.: Climate Sensitivity of Franz Josef Glacier, New Zealand, as Revealed by  
35 Numerical Modeling, *Arct. Alp. Res.*, 29(2), 233–239, 1997.
- 36 Oerlemans, J.: Extracting a climate signal from 169 glacier records, *Science*, 308(5722), 675–  
37 7, doi:10.1126/science.1107046, 2005.

- 1 Oerlemans, J.: The Microclimate of Valley Glaciers, Igitur, Utrecht University, 2010.
- 2 Oerlemans, J. and Knap, W. H.: A 1 year record of global radiation and albedo in the  
3 ablationzone of Morteratschgletscher, Switzerland, *J. Glaciol.*, 44(147), 231–238, 1998.
- 4 Oerlemans, J., Giesen, R. H. and Van den Broeke, M. R.: Retreating alpine glaciers: increased  
5 melt rates due to accumulation of dust (Vadret da Morteratsch, Switzerland), *J. Glaciol.*,  
6 55(192), 729–736, doi:10.3189/002214309789470969, 2009.
- 7 Pellicciotti, F., Brock, B., Strasser, U., Burlando, P., Funk, M. and Corripio, J.: An enhanced  
8 temperature-index glacier melt model including the shortwave radiation balance: development  
9 and testing for Haut Glacier d’Arolla, Switzerland, *J. Glaciol.*, 51(175), 573–587,  
10 doi:10.3189/172756505781829124, 2005.
- 11 Peltier, W. R. and Marshall, S.: Coupled energy balance/ice-sheet model simulations of the  
12 glacial cycle: A possible connection between terminus and terrigenous dust, *J. Geophys. Res.*,  
13 100(D7), 14,269–14,289, 1995.
- 14 Putnam, A. E., Schaefer, J. M., Denton, G. H., Barrell, D. J. A., Finkel, R. C., Andersen, B.  
15 G., Schwartz, R., Chinn, T. J. H. and Doughty, A. M.: Regional climate control of glaciers in  
16 New Zealand and Europe during the pre-industrial Holocene, *Nat. Geosci.*, 5(9), 627–630,  
17 doi:10.1038/ngeo1548, 2012.
- 18 Sicart, J. E., Hock, R. and Six, D.: Glacier melt, air temperature, and energy balance in  
19 different climates: The Bolivian Tropics, the French Alps, and northern Sweden, *J. Geophys.*  
20 *Res.*, 113(D24), D24113, doi:10.1029/2008JD010406, 2008.
- 21 Sicart, J. E., Hock, R., Ribstein, P. and Chazarin, J. P.: Sky longwave radiation on tropical  
22 Andean glaciers : parameterization and sensitivity to atmospheric variables, *J. Glaciol.*,  
23 56(199), 854–860, 2010.
- 24 Tait, A. B. and Fitzharris, B. B.: Relationships between New Zealand rainfall and south-west  
25 Pacific pressure patterns, *Int. J. Climatol.*, 18(4), 407–424, doi:10.1002/(SICI)1097-  
26 0088(19980330)18:4<407::AID-JOC256>3.0.CO;2-S, 1998.
- 27 Uddstrom, M. J., McGregor, J. A., Gray, W. R. and Kidson, J. W.: A High-Resolution  
28 Analysis of Cloud Amount and Type over Complex Topography, *J. Appl. Meteorol.*,  
29 40(2001), 16–33, 2001.
- 30 Ummenhofer, C. C. and England, M. H.: Interannual Extremes in New Zealand Precipitation  
31 Linked to Modes of Southern Hemisphere Climate Variability, *J. Clim.*, 20(21), 5418–5440,  
32 doi:10.1175/2007JCLI1430.1, 2007.
- 33 Van Den Broeke, M. R., Van As, D., Reijmer, C. and Van de Wal, R.: Assessing and  
34 Improving the Quality of Unattended Radiation Observations in Antarctica, *J. Atmos. Ocean.*  
35 *Technol.*, 21(9), 1417–1431, doi:10.1175/1520-0426(2004)021<1417:AAITQO>2.0.CO;2,  
36 2004.

- 1 Van den Broeke, M., Reijmer, C., Van As, D. and Boot, W.: Daily cycle of the surface energy  
2 balance in Antarctica and the influence of clouds, *Int. J. Climatol.*, 26(12), 1587–1605,  
3 doi:10.1002/joc.1323, 2006.
- 4 Van den Broeke, M. R., Smeets, C. J. P. P., Ettema, J. and Kuipers Munneke, P.: Surface  
5 radiation balance in the ablation zone of the west Greenland ice sheet, *J. Geophys. Res.*,  
6 113(D13), D13105, doi:10.1029/2007JD009283, 2008a.
- 7 Van den Broeke, M. R., Smeets, C. J. P. P., Ettema, J., Van der Veen, C., Van de Wal, R. and  
8 Oerlemans, J.: Partitioning of melt energy and meltwater fluxes in the ablation zone of the  
9 west Greenland ice sheet, *Cryosph.*, 2(4), 711–736, doi:10.5194/tcd-2-711-2008, 2008b.
- 10 Van den Broeke, M. R., Smeets, C. J. P. P. and van de Wal, R. S. W.: The seasonal cycle and  
11 interannual variability of surface energy balance and melt in the ablation zone of the west  
12 Greenland ice sheet, *Cryosph.*, 5(2), 377–390, doi:10.5194/tc-5-377-2011, 2011.
- 13 Willis, I., Lawson, W., Owens, I., Jacobel, B. and Autridge, J.: Subglacial drainage system  
14 structure and morphology of Brewster Glacier, New Zealand, *Hydrol. Process.*, 23, 384–396,  
15 doi: 10.1002/hyp.7146, 2009.
- 16
- 17

1 **Tables**

2

3 **Table 1.** Variables measured, sensor specifications and mean annual values at AWS<sub>glacier</sub>.

<i>Variable</i>	<i>Instrument</i>	<i>Accuracy</i>	<i>Mean annual value</i>
Air temperature ( $T_a$ )	Vaisala HMP 45AC	0.3 °C	1.2 °C
Relative humidity ( $RH$ )	Vaisala HMP 45AC	3%	78%
Wind speed ( $U$ )	RM Young 01503	0.3 m s <sup>-1</sup>	3.3 m s <sup>-1</sup>
Atmospheric pressure ( $p$ )	Vaisala PTB110	0.5 hPa	819 hPa
Incoming shortwave radiation ( $SW_{\downarrow, meas}$ )	Kipp and Zonen CNR4	5%*	140 W m <sup>-2</sup>
Outgoing shortwave radiation ( $SW_{\uparrow}$ )	Kipp and Zonen CNR4	5%*	93 W m <sup>-2</sup>
Incoming longwave radiation ( $LW_{\downarrow, meas}$ )	Kipp and Zonen CNR4	5%*	278 W m <sup>-2</sup>
Surface temperature ( $T_s$ )	Kipp and Zonen CNR4	1°C**	-2.7 °C
Precipitation ( $P_{scaled}$ )***	<i>TB4 + Scaled</i> ***	25%***	6125 mm***
Surface and sensor height	SR50a	±1 cm	n/a

4 \* Uncertainty is estimated to be less than the manufacturer's specifications as noted in van den  
5 Broeke et al. (2004) and Blonquist et al. (2009).

6 \*\* Based on a 5 W m<sup>-2</sup> uncertainty in outgoing longwave radiation.

7 \*\*\* From AWS<sub>lake</sub> during snow free period only.  $P_{scaled}$  is based on scaled relationship between AWS<sub>lake</sub>  
8 and a lowland station (Cullen and Conway, 2015). Uncertainty is estimated from fit of scaled  
9 relationship.

10

11

12

1 **Table 2.** Configuration of SEBmr and SEBpr, showing input data and references used in the  
 2 calculation of radiation terms in each configuration.

Variable	Model version	Reference and /or input data
$\alpha$	SEBmr	Accumulated albedo (van den Broeke et al., 2004)
	SEBpr	Oerlemans and Knap (1998) ( $P_{scaled}$ , $T_a$ )
$SW_{\downarrow}$	SEBmr	$SW_{\downarrow surface}$
	SEBpr	Conway et al., 2014 ( $N_{\epsilon}$ , $T_a$ , $RH$ )
$LW_{\downarrow}$	SEBmr	$LW_{\downarrow meas}$
	SEBpr	Conway et al., 2014 ( $N_{\epsilon}$ , $T_a$ , $RH$ )

3

4

5

1 **Table 3.** Input parameter uncertainty introduced in Monte Carlo simulations of SMB  
 2 uncertainty.

Input parameter	Value(s)	Systematic [random] error	Model
Roughness length for momentum ( $z_{0v}$ ) <sup>a</sup>	$3.6 \times 10^{-3}$ m	$z_{0v} \times$ $10^{\wedge}$ NORMRND(0,0.274)	SEBmr,pr
Rain/snow threshold ( $T_{r/s}$ ) <sup>b</sup>	1.0 °C	0.3 [0.5]	SEBmr,pr
Albedo of surface ( $\alpha_{snow}$ , $\alpha_{firm}$ , $\alpha_{ice}$ ) <sup>b</sup>	0.95 ( $\alpha_{snow}$ ) 0.65 ( $\alpha_{firm}$ ) 0.42 ( $\alpha_{ice}$ )	0.05	SEBpr
Constant for cloud extinction coefficient <sup>c</sup>	0.1715	0.0048 [0.0048]	SEBpr
Multiplier for cloud extinction coefficient <sup>c</sup>	0.07182 hPa <sup>-1</sup>	0.0324 [0.0324]	SEBpr
Albedo of surrounding terrain <sup>d</sup>	0.45	0.1	SEBpr
Clear-sky emissivity constant <sup>e</sup>	0.456 Pa <sup>-1</sup> K	0.0204 [0.0204]	SEBpr

3 <sup>a</sup> standard deviation of  $z_{0v}$  (Conway and Cullen, 2013). NORMRND is a MATLAB function that selects  
 4 a random number from a normal distribution with mean of 0 and standard deviation of 0.274

5 <sup>b</sup> Macguth et al. (2008)

6 <sup>c</sup> 95% confidence interval of optimised coefficients (Conway et al., 2015). Limited to 0.95

7 <sup>d</sup> Assumed; no random errors as terrain albedo will not vary at this timescale (30 minutes)

8 <sup>e</sup> RMSD of clear-sky values (Conway et al., 2015)

9

10

11

1 **Table 4.** Observed and modelled SMB (m w.e) for selected periods between stake  
2 measurements in ablation (Abl) and accumulation (Acc) seasons. Figure 4 shows the length  
3 of each period.

Period	Observed	SEBmr	SEBpr
Abl1 snow	-1.74	-1.78	-1.67
Abl1 ice	-3.35	-2.92	-3.28
Acc1	1.52	1.40	1.46
Abl2 snow	-1.51	-1.78	-1.48
Abl2 ice	-1.94	-1.87	-1.66

4

5

6

- 1 **Table 5.** Mean differences in surface climate between clear-sky and overcast conditions.  
 2 Positive values indicate an increase in overcast conditions.

Variable	Jan	Feb	Mar	Apr	May	Jun	Jul	Aug	Sep	Oct	Nov	Dec	Annual
$T_a$ (°C)	<b>-1.3</b>	-0.2	<b>-0.8</b>	<b>-3</b>	<b>-0.9</b>	<b>-0.5</b>	<b>-1.3</b>	<b>-1.2</b>	<b>-0.7</b>	-0.1	<b>-1.4</b>	<b>-1.2</b>	<i>-1.1</i>
$RH$ (%)	<b>35</b>	<b>25</b>	<b>35</b>	<b>53</b>	<b>44</b>	<b>39</b>	<b>52</b>	<b>37</b>	<b>45</b>	<b>33</b>	<b>34</b>	<b>37</b>	39
$e_a$ (hPa)	<b>2.5</b>	<b>2.2</b>	<b>2.5</b>	<b>3.1</b>	<b>2.6</b>	<b>2.2</b>	<b>2.6</b>	<b>1.7</b>	<b>2.3</b>	<b>2.1</b>	<b>2</b>	<b>2.7</b>	<i>2.4</i>
$U$ (m s <sup>-1</sup> )	<b>0.6</b>	0.1	<b>0.6</b>	<b>-0.2</b>	<b>-0.1</b>	0	0	<b>-0.2</b>	-0.1	-0.1	<b>0.2</b>	<b>0.7</b>	<i>0.1</i>
$T_s$ (°C)	<b>0.5</b>	<b>0.3</b>	<b>0.9</b>	<b>1.5</b>	<b>4.7</b>	<b>5.4</b>	<b>6.3</b>	<b>5.2</b>	<b>5.8</b>	<b>2.6</b>	<b>1.5</b>	<b>0.6</b>	<i>2.9</i>
$p$ (hPa)	<b>-7</b>	<b>-4</b>	<b>-8</b>	<b>-6</b>	<b>-10</b>	<b>-7</b>	<b>-12</b>	<b>-4</b>	<b>-9</b>	<b>-3</b>	<b>-7</b>	<b>-8</b>	<i>-7</i>

- 3 Bold face indicates monthly differences are significant at the 95% level using a two sided t-test assuming unequal  
 4 variances. Temperature and wind speed are normalised to 2-metre values.

- 5  
 6  
 7

1 **Table 6.** Average surface energy fluxes ( $\text{W m}^{-2}$ ) for melting periods in clear-sky and overcast  
 2 conditions, all melting periods, and all periods during the measurement period. Bracketed  
 3 italics show the proportion of *QM* for each condition.

	<i>SWnet</i>	<i>LWnet</i>	<i>Rnet</i>	<i>QS</i>	<i>QL</i>	<i>QR</i>	<i>QC</i>	<i>QM</i>
Melting + clear-sky periods	240 ( <i>121</i> )	-67 ( <i>-34</i> )	173 ( <i>87</i> )	39 ( <i>20</i> )	-7 ( <i>-3</i> )	0 ( <i>0</i> )	-6 ( <i>-3</i> )	199
Melting + overcast periods	36 ( <i>33</i> )	15 ( <i>14</i> )	51 ( <i>46</i> )	30 ( <i>27</i> )	24 ( <i>22</i> )	7 ( <i>7</i> )	-2 ( <i>-2</i> )	110
Melting periods	96 ( <i>70</i> )	-8 ( <i>-6</i> )	88 ( <i>65</i> )	32 ( <i>24</i> )	15 ( <i>11</i> )	5 ( <i>3</i> )	-3 ( <i>-2</i> )	136
All periods	49 ( <i>83</i> )	-27 ( <i>-46</i> )	22 ( <i>37</i> )	31 ( <i>53</i> )	2 ( <i>3</i> )	2 ( <i>4</i> )	2 ( <i>3</i> )	58

4 Melting conditions are selected as periods where *QM* > 0 in SEBmr.

5

1 **Table 7.**  $\Delta$ SMB (mm w.e. yr<sup>-1</sup>) to perturbations in surface climate and shortwave radiation  
2 terms. While the values shown are the average change in SMB per year for both positive and  
3 negative perturbations in each climate variable, for clarity,  $\Delta$ SMB is expressed as the SMB  
4 response to an increase in a given input variable or parameter.

Variable and perturbation	$\Delta$ SMB
$T_a + 1$ K	- 2065
$P_{scaled} + 20\%$	+ 770
$RH + 10\%$	- 380
$U + 1$ m s <sup>-1</sup>	- 790
$\alpha + 0.1$	+ 1220
<i>Solar constant</i> - 6%	- 260
$k + 0.17$	- 740

5

6

7

1 **Table 8** Cumulative sum of SMB terms for selected runs of SEBpr over the two year  
 2 sensitivity period. All units are in mm w.e., except for  $\Delta$  which is in mm w.e. K<sup>-1</sup> yr<sup>-1</sup>.

Scenario	SMB	Snowfall	Melt	Sublimation	Deposition	Refreezing
+1 K	-9181	3900	13064	32	134	85
- 1 K	-920	5670	6692	38	135	198
$\Delta$ (mm w.e. K <sup>-1</sup> yr <sup>-1</sup> )	-2065	443	-1593	2	0	28

3

4

1 **Table 9.** Mean SEB terms ( $W m^{-2}$ ) during melting periods in the +1 K (A) and -1 K (B)  
2 perturbation runs of SEBpr. Also shown are mean SEB terms ( $W m^{-2}$ ) in the -1 K perturbation  
3 run, for the same periods as A, i.e. melting periods in the +1 K perturbation run (C), and the  
4 increases ( $W m^{-2}$ ) between each scenario (D, E). The percentage contribution of each flux to  
5  $QM$ , or the increase in  $QM$ , is given in bracketed italics. The percentage contribution of each  
6 flux to  $\Delta SMB$  is given in the last row (F)

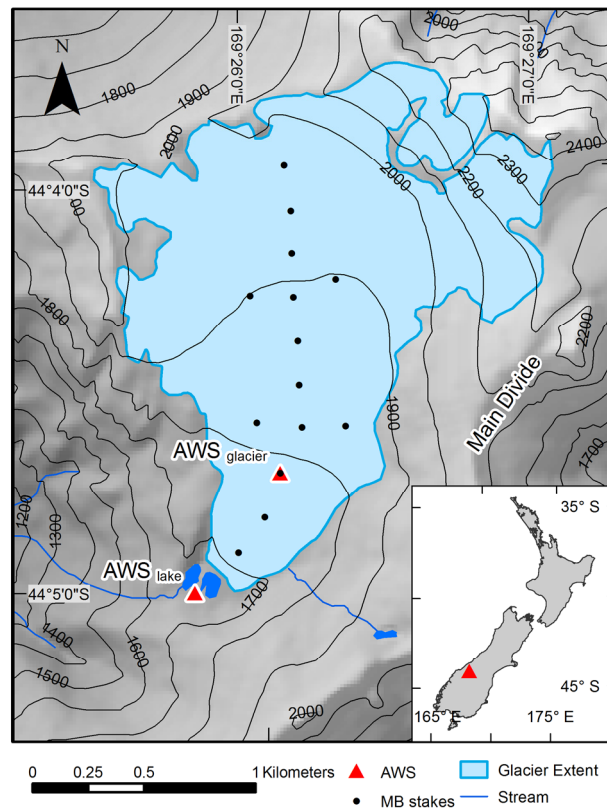
Scenario	<i>SWnet</i>	<i>LWnet</i>	<i>Rnet</i>	<i>QS</i>	<i>QL</i>	<i>QR</i>	<i>QC</i>	<i>QM</i>
A: +1 K melting periods	89 (62)	-4 (-3)	85 (59)	37 (26)	19 (14)	5 (3)	-2 (-1)	144
B: -1 K melting periods	70 (68)	-9 (-8)	61 (60)	28 (27)	11 (11)	4 (4)	-2 (-2)	103
C: -1 K for same periods as A	56 (76)	-13 (-17)	43 (59)	23 (32)	7 (9)	3 (4)	-2 (-2)	74
D: Increase from B to A	19 (46)	5 (11)	23 (57)	9 (22)	8 (20)	1 (2)	0 (0)	41
E: Increase from C to A	33 (47)	8 (12)	41 (59)	14 (20)	13 (18)	2 (3)	0 (0)	70
F: Contribution to $\Delta SMB$	36%	9%	45%	15%	14%	2%	0%	77%

7

8

1 **Figures**

2



3

4 **Fig. 1.** Map of Brewster Glacier showing AWS locations and surrounding topography.

5 Contour lines are at 100 m intervals. Long-term mass balance network (MB stakes) shown

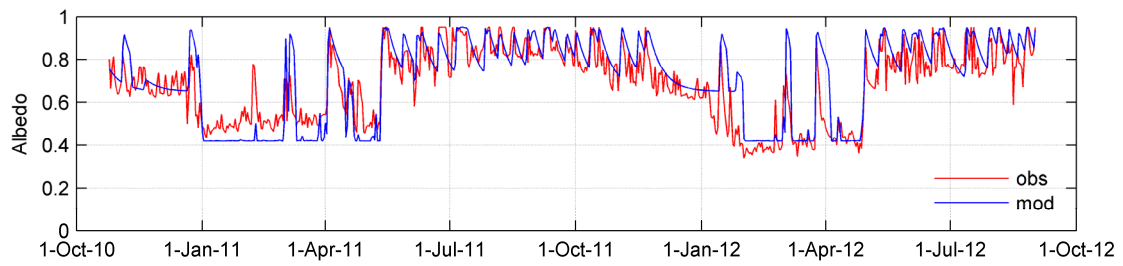
6 as filled circles. The glacier margin shown is based on a 1997 GPS survey (Willis et al.,

7 2009). The ridgeline to the southeast of the glacier is the main divide of the Southern Alps.

8 The inset map shows the location of Brewster Glacier within New Zealand.

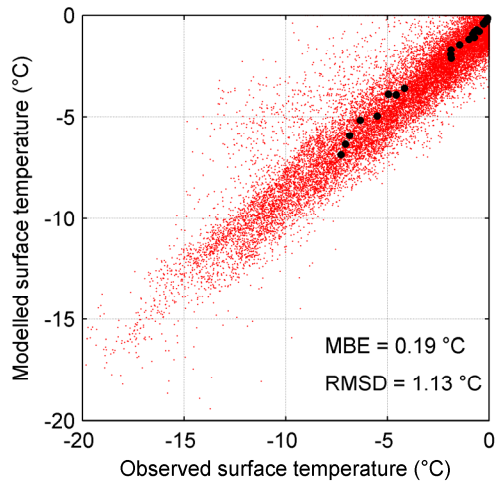
9

10

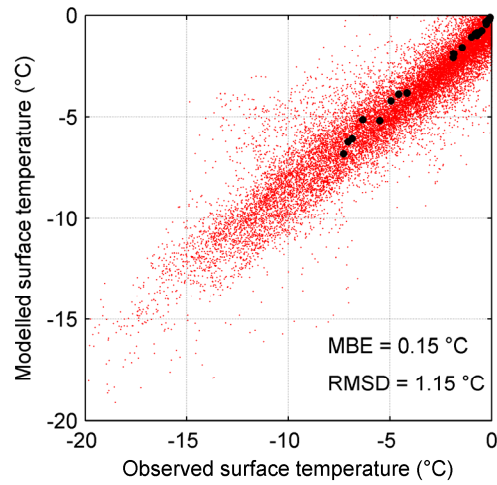


1  
2  
3  
4  
5  
6  
7

**Fig. 2.** Daily average albedo observed at AWSglacier (red) during the measurement period and modelled in SEBpr (blue) using the expressions of Oerlemans and Knap (1998), with locally optimised coefficients.



(a) SEBmr



(b) SEBpr

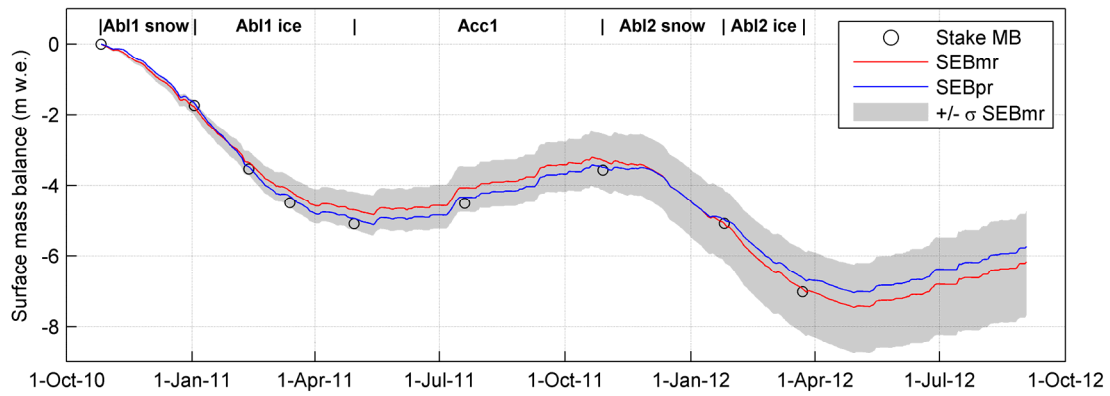
1

2 **Fig. 3.** Observed versus modelled surface temperature for (a) SEBmr and (b) SEBpr runs.

3 Red dots are 30-minute averages, while black dots are monthly averages.

4

1

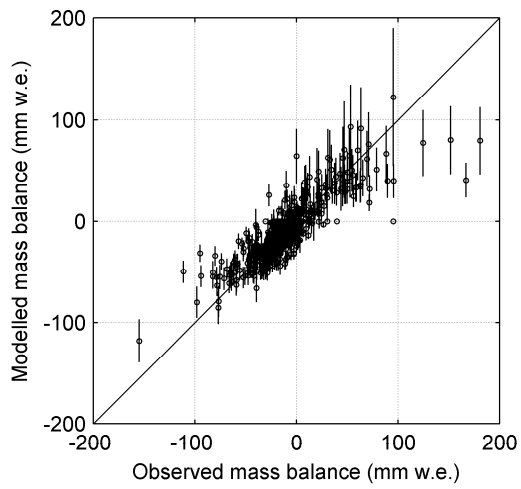


2

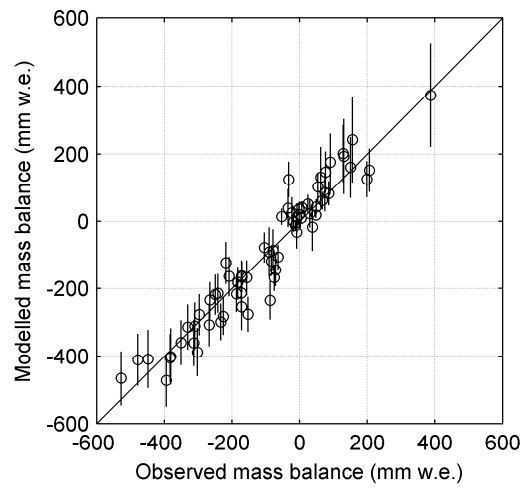
3 **Fig. 4** Accumulated SMB during the measurement period as modelled by the reference runs  
4 of SEBmr and SEBpr. The points give observed mass balance from periodic stake and snow  
5 pit measurements. The SMB for selected ablation and accumulation periods (shown as Abl1  
6 snow etc.) are given in Table 4. The shaded envelope shows  $\pm 1$  standard deviation from the  
7 mean of SEBmr, calculated using Monte Carlo simulations (see Sect. 2.4 for details).

8

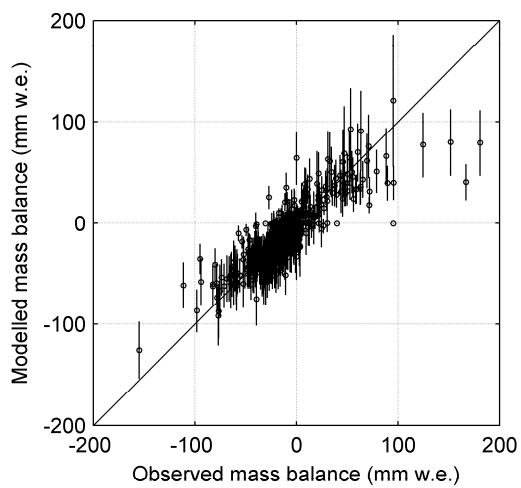
1  
2



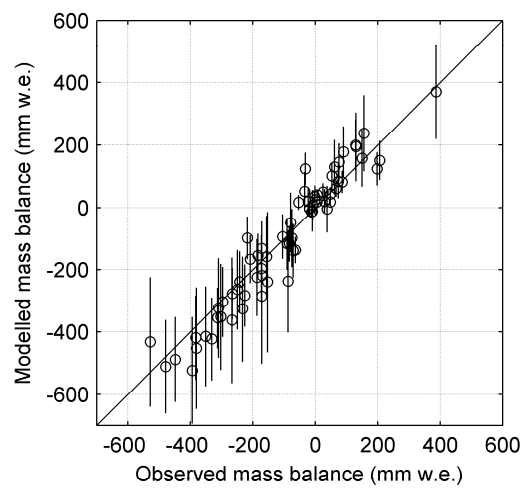
(a) SEBmr: Daily totals



(b) SEBmr: 10-day totals



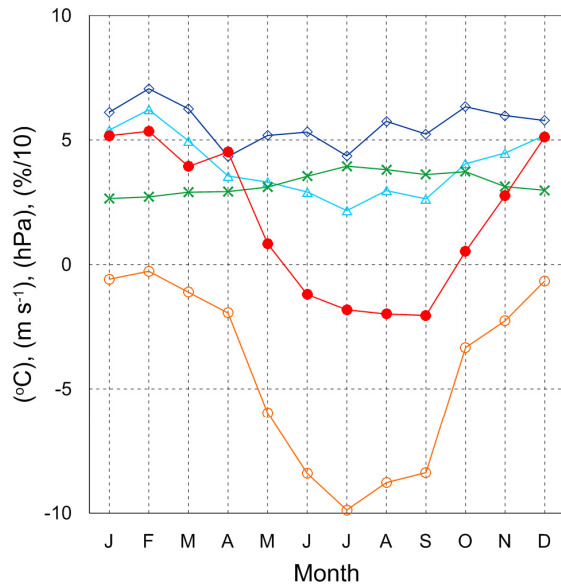
(c) SEBpr: Daily totals



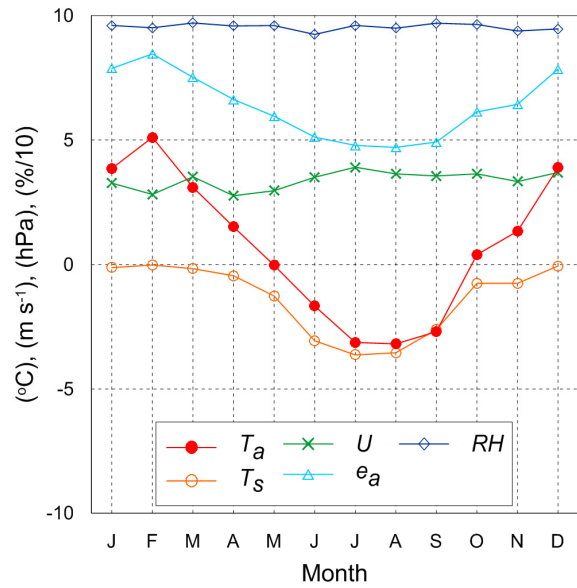
(d) SEBpr: 10-day totals

3  
4  
5  
6  
7  
8

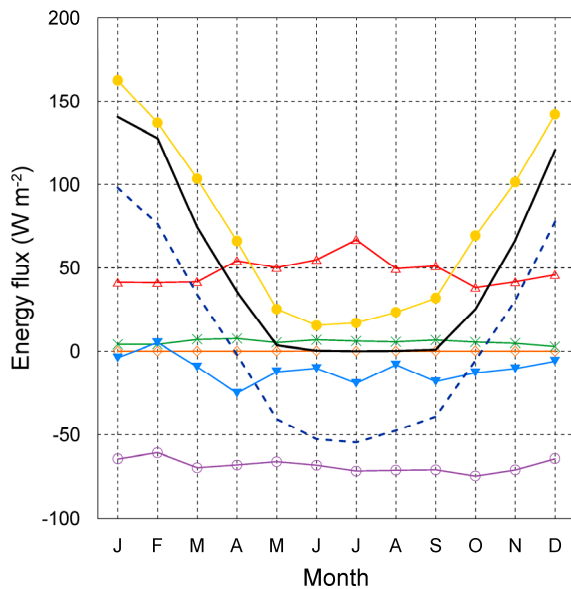
**Fig. 5.** Observed versus modelled mass balance for (a, b) SEBmr and (c, d) SEBpr over 1-day and 10-day periods. Error bars show  $\pm 2 \sigma$  from the ensemble mean values. The solid diagonal line is a 1:1 line.



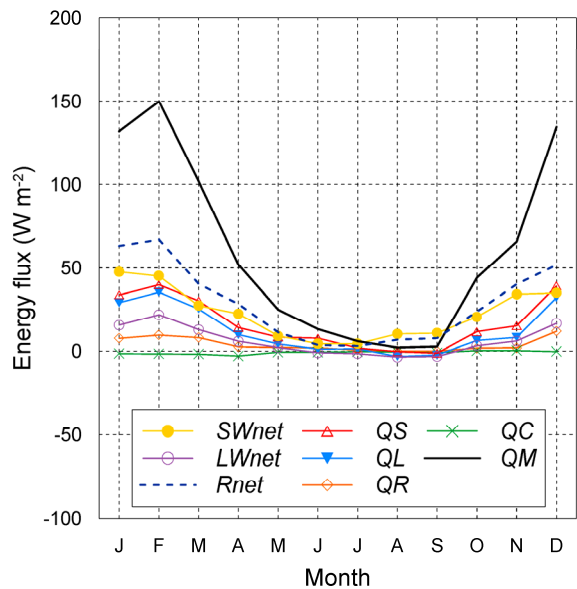
(a) clear-sky



(b) overcast

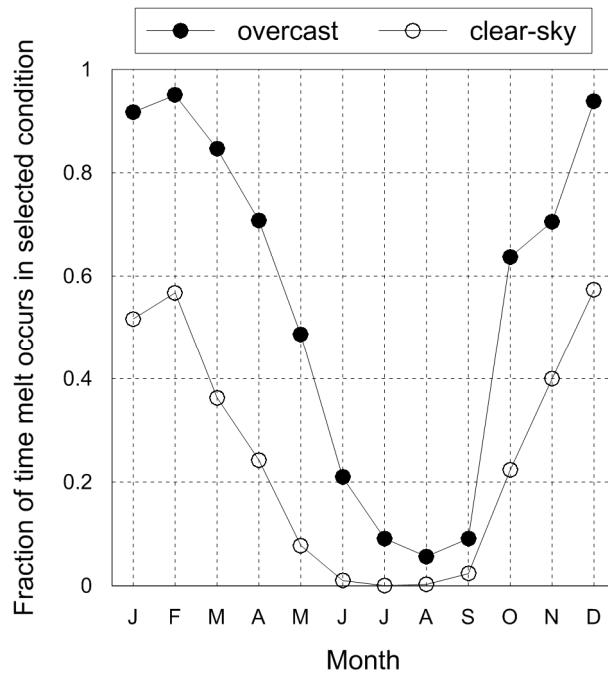


(c) clear-sky



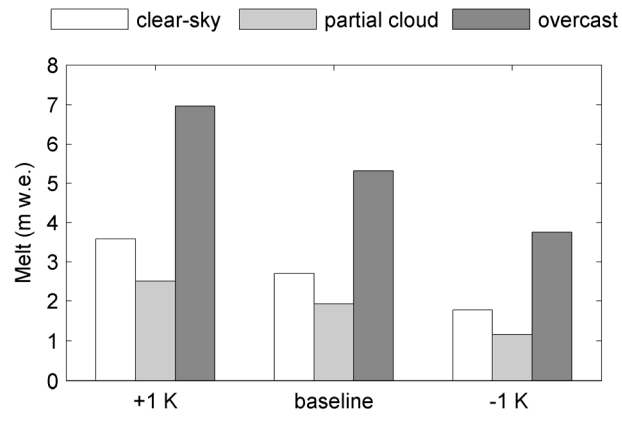
(d) overcast

**Fig. 6.** Monthly mean surface climate (a, b) and surface energy fluxes (c, d) at AWS<sub>glacier</sub> in (a, c) clear-sky and (b, d) overcast conditions. Partial cloud conditions are a graduation between the two extremes and are not shown for brevity. Surface climate variables include air and surface temperature ( $T_a$  and  $T_s$ ; °C), wind speed ( $U$ ; m s<sup>-1</sup>), vapour pressure ( $e_a$ ; hPa), and relative humidity ( $RH$ ) on a scale from 0 to 10 (i.e. %/10).



1  
 2 **Fig. 7.** Fraction of time surface melting occurred in clear-sky (open circles) and overcast  
 3 (closed circles) conditions during each month. Melting conditions are selected as periods  
 4 where  $QM > 0$  in SEBmr.

5  
 6

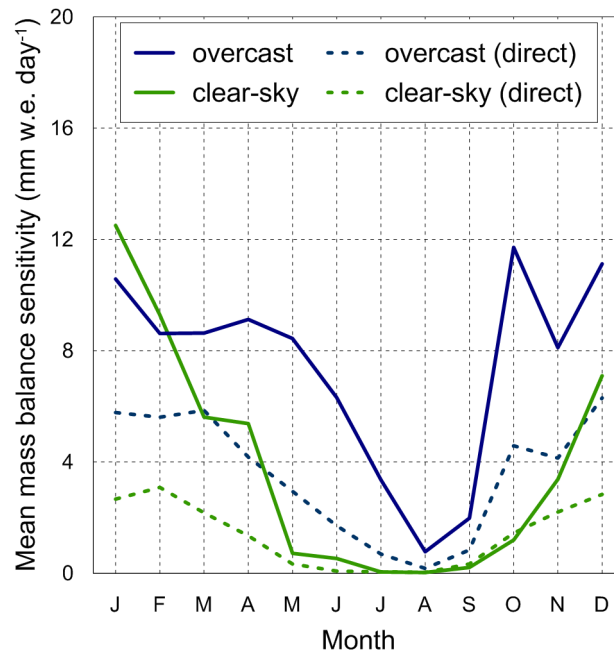


1

2 **Fig. 8.** Total surface melt in each cloud cover category for baseline and climate perturbation  
3 scenarios.

4

1



2

3 **Fig. 9.** The mean daily mass balance sensitivity ( $\Delta\text{SMB}$ ) to a 1 K change in  $T_a$ , separated  
4 into clear-sky (green) and overcast (blue) conditions, in each month of the year. The dashed  
5 lines show  $\Delta\text{SMB}$  resulting from only a direct change in  $QM$ , which was derived from a  
6 further model run using measured albedo and perturbing  $T_{r/s}$  with  $T_a$ . The positive values  
7 indicate mass loss for increased  $T_a$ .